



Central Mediterranean tephrochronology between 313 and 366 ka: New insights from the Fucino palaeolake sediment succession

NIKLAS LEICHER , BIAGIO GIACCIO, ALISON PEREIRA, SEBASTIEN NOMADE, LORENZO MONACO, GIORGIO MANNELLA, PAOLO GALLI, EDOARDO PERONANCE, DANILO MAURO PALLADINO, GIANLUCA SOTTILI, GIOVANNI ZANCHETTA AND BERND WAGNER 

BOREAS



Leicher, N., Giaccio, B., Pereira, A., Nomade, S., Monaco, L., Mannella, G., Galli, P., Peronance, E., Palladino, D. M., Sottili, G., Zanchetta, G. & Wagner, B. 2023 (April): Central Mediterranean tephrochronology between 313 and 366 ka: New insights from the Fucino palaeolake sediment succession. *Boreas*, Vol. 52, pp. 240–271. <https://doi.org/10.1111/bor.12610>. ISSN 0300-9483.

Thirty-two tephra layers were identified in the time-interval 313–366 ka (Marine Isotope Stages 9–10) of the Quaternary lacustrine succession of the Fucino Basin, central Italy. Twenty-seven of these tephra layers yielded suitable geochemical material to explore their volcanic origins. Investigations also included the acquisition of geochemical data of some relevant, chronologically compatible proximal units from Italian volcanoes. The record contains tephra from some well-known eruptions and eruptive sequences of Roman and Roccamonfina volcanoes, such as the Magliano Romano Plinian Fall, the Orvieto–Bagnoregio Ignimbrite, the Lower White Trachytic Tuff and the Brown Leucitic Tuff. In addition, the record documents eruptions currently undescribed in proximal (i.e. near-vent) sections, suggesting a more complex history of the major eruptions of the Colli Albani, Sabatini, Vulsini and Roccamonfina volcanoes between 313 and 366 ka. Six of the investigated tephra layers were directly dated by single-crystal-fusion $^{40}\text{Ar}/^{39}\text{Ar}$ dating, providing the basis for a Bayesian age–depth model and a reassessment of the chronologies for both already known and dated eruptive units and for so far undated eruptions. The results provide a significant contribution for improving knowledge on the peri-Tyrrhenian explosive activity as well as for extending the Mediterranean tephrostratigraphical framework, which was previously based on limited proximal and distal archives for that time interval.

Niklas Leicher (n.leicher@uni-koeln.de) and Bernd Wagner, Institute of Geology and Mineralogy, University of Cologne, Zùlpicher Straße 49a, 50674 Cologne, Germany; Biagio Giaccio, Istituto di Geologia Ambientale e Geoingegneria, CNR, Area della Ricerca di Roma 1 Strada Provinciale 35d, 9-00010 Montelibretti, Italy and Istituto Nazionale di Geofisica e Vulcanologia, Via di Vigna Murata 605, 00143 Rome, Italy; Sebastien Nomade: Laboratoire des Sciences du Climat et de l'Environnement, LSCE/IPSU, UMR 8212, CEA-CNRS-UVSQ, Université Paris-Saclay, F-91190 Gif-sur-Yvette, France; Alison Pereira, Laboratoire Géosciences Paris-Saclay (GEOPS), UMR 8148, Université Paris-Saclay, F-91450 Orsay, France; Lorenzo Monaco, Istituto di Geologia Ambientale e Geoingegneria, CNR, Area della Ricerca di Roma 1 - Strada Provinciale 35d, 9-00010 Montelibretti, Italy and Dipartimento di Scienze della Terra, University of Pisa, Via Santa Maria 53, 56126 Pisa, Italy; Giorgio Mannella and Giovanni Zanchetta, Dipartimento di Scienze della Terra, University of Pisa, Via Santa Maria 53, 56126 Pisa, Italy; Paolo Galli, Istituto di Geologia Ambientale e Geoingegneria, CNR, Area della Ricerca di Roma 1 - Strada Provinciale 35d, 9-00010 Montelibretti, Italy and Dipartimento di Protezione Civile, Via Vitorchiano 4, 00189 Rome, Italy; Edoardo Peronance, Istituto di Geologia Ambientale e Geoingegneria, CNR, Area della Ricerca di Roma 1 - Strada Provinciale 35d, 9-00010 Montelibretti, Italy; Danilo M. Palladino and Gianluca Sottili, Dipartimento di Scienze della Terra, Sapienza Università di Roma, Piazzale Aldo Moro 5, 00185 Rome, Italy; received 4th July 2022, accepted 4th November 2022.

The intense and persistent Middle to Upper Pleistocene explosive volcanism in the central and eastern Mediterranean region entailed the widespread dispersal of volcanic ash and thus deposition in numerous sedimentary archives. Hence, this region provides favourable conditions for tephrostratigraphical and tephrochronological studies. The first detailed tephrostratigraphical framework based on marine sediment successions was established in the Mediterranean region in the 1970s (Keller *et al.* 1978) and has been continuously refined since then by including terrestrial sequences (e.g. Paterne *et al.* 1988, 2008; Narcisi & Vezzoli 1999; Wulf *et al.* 2004, 2008, 2012; Calanchi & Dinelli 2008; Albert *et al.* 2012; Tamburrino *et al.* 2012, 2016; Giaccio *et al.* 2013a; Insinga *et al.* 2014; Petrosino *et al.* 2014, 2019; Bourne *et al.* 2015; Zanchetta *et al.* 2019). Tephrostratigraphical and tephrochronological studies in the Mediterranean are often applied for chronological purposes within the scope of palaeoenvironmental, palaeoclimatic and/or

archaeological investigations (e.g. Zanchetta *et al.* 2016; Lane *et al.* 2017; Wagner *et al.* 2019, 2022). The applicability and reliability of this dating-correlation tool depends on the completeness and the quality of the reference geochemical and geochronological dataset, which in turn requires integration of investigations of both near-vent and distal tephra, an approach that has also proven crucial for assessing the frequency of eruptions and associated volcanic hazards (e.g. Sulpizio *et al.* 2014; Albert *et al.* 2019; Monaco *et al.* 2021).

Both the completeness of explosive volcanic eruption stratigraphies and the availability of geochemical and precise and accurate chronological data of the Mediterranean tephrostratigraphical framework differ throughout the Quaternary. Single distal archives have pushed the overall framework for the central Mediterranean back in time, such as Lake Ohrid to *c.* 1.3 Ma (Leicher *et al.* 2021), the Tenaghi Philippon peat record to *c.* 460 ka (Vakhrameeva *et al.* 2018, 2019; Wulf *et al.* 2018)

and the Ionian Sea record ODP964 to *c.* 800 ka (Vakhrameeva *et al.* 2021). However, only specific time intervals older than 200 ka were studied in a few records at high resolution (Giaccio *et al.* 2014, 2015a, 2021; Vakhrameeva *et al.* 2018, 2019; Pereira *et al.* 2020; Monaco *et al.* 2021, 2022b). Records in proximity to the peri-Tyrrhenian volcanoes indicate frequent volcanic activity with powerful eruptions during the period 200–370 ka (Rouchon *et al.* 2008; Sottili *et al.* 2010; Palladino *et al.* 2014; Marra *et al.* 2020a, b, 2021b). Unfortunately, near-vent proximal archives are often discontinuous and incomplete, especially for the older activity, because of subaerial processes (pedogenetic, erosional) and burial by subsequent younger volcanic activity, as demonstrated by numerous eruptions identified only in distal archives (Giaccio *et al.* 2014; Petrosino *et al.* 2014, 2019; Leicher *et al.* 2021; Vakhrameeva *et al.* 2021). Long and continuous distal records can provide a more complete stratigraphical order of the peri-Tyrrhenian volcanic activity between 200 and 370 ka. Combining proximal volcanological information with distal sedimentary records allows the assessment of the relative (climato-) stratigraphic position of prominent eruptions and the integration of existing eruptive ages and newly identified eruptions into the tephrostratigraphical framework. This is crucial to extend the understanding of the history of peri-Tyrrhenian volcanic provinces as well as the activities of individual volcanic centres. Further, identifying these eruptions within palaeoenvironmental records would allow determination of their climatostratigraphical position, which can then be used to investigate leads and lags of spatial and temporal environmental change (e.g. Blockley *et al.* 2014; Regattieri *et al.* 2015; Zanchetta *et al.* 2016; Giaccio *et al.* 2021). Equivalent of known eruptions in the period 200–370 ka are currently only partially identified in distal archives (Vakhrameeva *et al.* 2018, 2021; Leicher *et al.* 2019). A comprehensive and continuous high-resolution tephrostratigraphical record covering this period comes from the Fucino Basin in central Italy. Its tectonic evolution allowed the deposition of a continuous sedimentary succession recording past environmental and climatic changes. Moreover, its geographical position in a good range (i.e. ~50–200 km) downwind of most volcanic systems from central Italy makes it a cornerstone to study proximal and distal tephra deposits. Previous drillings in the Fucino Basin have demonstrated the exceptional potential of the record for the last 190 ka (F1–F3 record, FUC S5–6; Giaccio *et al.* 2017a; Di Roberto *et al.* 2018; Mannella *et al.* 2019; Del Carlo *et al.* 2020). The F4–F5 record was drilled in 2017 and covers the last *c.* 425 ka (Giaccio *et al.* 2019). Recent studies of this record already greatly improved the Mediterranean tephrostratigraphy for the intervals 366–425 ka (~MIS 11, Monaco *et al.* 2021) and 250–170 ka (~MIS 6–8, Monaco *et al.* 2022b). Here, the investigation of the F4–F5 record focuses on the period 313–366 ka (MIS 9–10), presenting

new geochemical and chronological data and their integration within the regional tephrostratigraphical framework.

Regional setting

Fucino Basin

The Fucino Basin (42°00′00″N; 013°30′00″E) is located ~650 m a.s.l. in the Abruzzo region in central Italy and is the largest extensional tectonic basin of the central-southern Apennine chain (Fig. 1A). The basin opened along E–W, NE–SW and NW–SE oriented faults (i.e. the Fucino Fault System, Fig. 1B) since the Late Pliocene to Early Pleistocene (e.g. Galadini & Galli 2000; D’Agostino *et al.* 2001; Giaccio *et al.* 2012; Amato *et al.* 2014). Seismic investigations of the Fucino Basin revealed a semi-graben architecture with an increasing sediment infill of up to ~900 m thickness from West towards the depocentre in the East (Patacca *et al.* 2008). The Plio-Quaternary deposits unconformably overlay both late Messinian terrigenous deposits and the Meso-Cenozoic carbonate basement (Cavinato *et al.* 2002; Giaccio *et al.* 2019; Mondati *et al.* 2021). The Plio-Pleistocene sedimentation is believed to have started before 2.0–3.0 Ma (Giaccio *et al.* 2015b; Mondati *et al.* 2021) and appears to be continuous, at least in the central part of the basin (Giaccio *et al.* 2017a, 2019; Mannella *et al.* 2019). The basin was constantly endorheic (Lanari *et al.* 2021) and hosted a lake (Lacus Fucinus) until it was artificially drained in historic times.

Peri-Tyrrhenian volcanic activity of the Middle Pleistocene

The Quaternary peri-Tyrrhenian volcanism includes the volcanic activity of the Roman Province (Vulsini, Vico, Sabatini and Colli Albani volcanic districts), the Roccamonfina Province, the Campanian Province (Neapolitan volcanoes of Somma–Vesuvius, Campi Flegrei, Ischia and Procida and the buried Campanian Plain volcanism), Mount Vulture, the Aeolian Arc, the Sicily Province and the Volsci Volcanic field (after Peccerillo & Frezzotti 2015; Cardello *et al.* 2020; see also Fig. 1C). For the period investigated here (313–366 ka), explosive volcanic activity is mainly known for the Roman and Roccamonfina Provinces and the Volsci Volcanic field (Fig. 1C). At the Vulsini Volcanic District (VVD) of the Roman Province, widespread activity is reported for the Vulsini Fields and Bolsena–Orvieto complexes between 320 and 380 ka (Palladino *et al.* 2010, 2014; Marra *et al.* 2020b). For the Vico volcano no eruptions are described between 305 and 390 ka (Perini *et al.* 2004; Monaco *et al.* 2021). The Sacrofano and Bracciano calderas of the Sabatini Volcanic District (SVD) were contemporaneously active between 200 and 330 ka (Sottili *et al.* 2010, 2019). The Tuscolano–Artemisio phase, or Vulcano Laziale period, of the Colli Albani

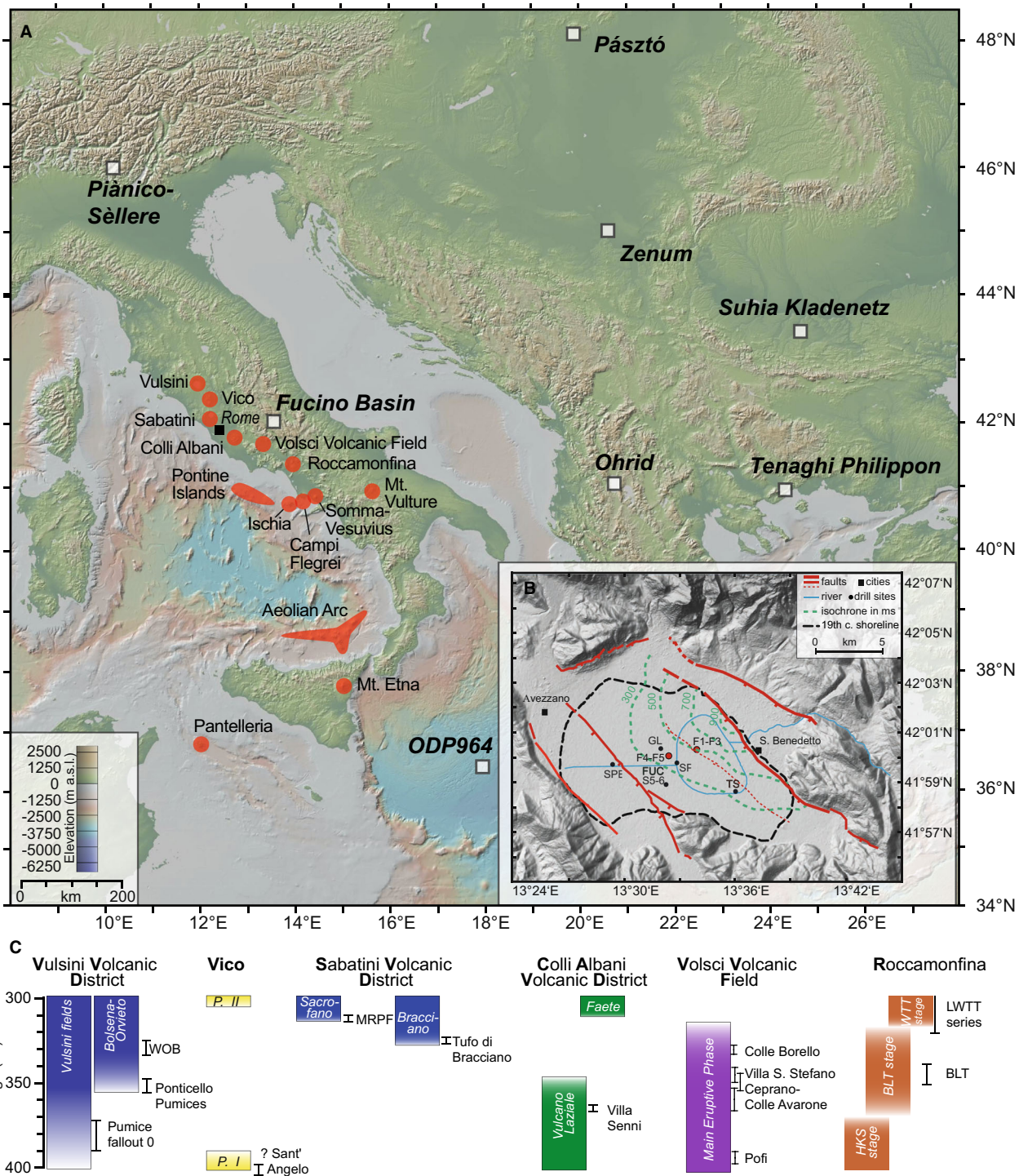


Fig. 1. A. Overview map of the central Mediterranean region and the location of Italian volcanoes (red circles) and archives discussed in the text (black squares). B. Map of the Fucino Basin and drill sites, main tectonic lines and sedimentary infill according to Cavinato *et al.* (2002). Maps made with GeoMapApp (www.geomapp.org) based on the Global Multi-Resolution Topography by Ryan *et al.* (2009). C. Overview of the known Italian volcanic activity of the Vulsini Volcanic District (VVD), Vico volcano, Sabatini Volcanic District (SVD), Colli Albani Volcanic District (CAVD), Volsci Volcanic Field (VVD) and Roccamonfina volcano for the period 300–400 ka. Active periods and active volcanic complexes (coloured bars, names in italics) are presented along with most prominent eruptions. The Aeolian Islands, Pantelleria, the Campanian Province (Ischia, Campi Flegrei, Somma Vesuvius) and Mt. Vulture are not shown, since no active phases are reported in proximal settings for the period studied. WOB = Orvieta–Bagnoregio eruption; P. I and P. II = Vico Period I and II; MRPF = Magliano Romano Plinian Fall; HKS = high K-series; BLT = Brown Leucitic Tuff; WTT = White Trachytic Tuff stage; LWTT = Lower White Trachytic Tuff. Data source for the Vulsini volcanic district: Palladino *et al.* (2010), Marra *et al.* (2019); for Vico: Perini *et al.* (2004); for the Monti Sabatini volcanic district: Marra *et al.* (2014), Sottili *et al.* (2004, 2010); for Colli Albani: Giaccio *et al.* (2013b); for Roccamonfina: Giannetti & De Casa (2000), Giannetti (2001), Rouchon *et al.* (2008); for the Volsci Volcanic Field: Marra *et al.* (2021a).

volcanic district (CAVD) terminates at *c.* 350 ka (Karner *et al.* 2001; Giordano *et al.* 2010; Giaccio *et al.* 2013b) followed by a *c.* 60-ka-long period of dormancy (Marra *et al.* 2016b). Within the Volsi Volcanic Field (VVF) the main eruptive phase occurred between 350 and 430 ka, potentially lasting until 330 ka (Marra *et al.* 2021a). At the Roccamonfina volcano, the Brown Leucitic Tuff (BLT) stage extended *c.* 400–350 ka, followed by the White Trachytic Tuff (WTT) stage at *c.* 330 ka, both including numerous eruptions (Rouchon *et al.* 2008). The oldest accessible volcanic products within the Campanian Province dates to *c.* 250 ka (Campanian Volcanic Zone of Rolandi *et al.* 2003; Belkin *et al.* 2016), but proximal well-log data (Brocchini *et al.* 2001) and ash layers preserved in distal archives suggest an older activity (Petrosino *et al.* 2014, 2015; Vakhrameeva *et al.* 2018, 2021; Leicher *et al.* 2019, 2021). At the Aeolian Islands the oldest proximal deposits date back to 270 ka (Forni *et al.* 2013), but evidence of older explosive eruptions is found in distal archives (Giaccio *et al.* 2014; Leicher *et al.* 2019; Vakhrameeva *et al.* 2019, 2021). Little is known about the activity of Mt Etna and Pantelleria of the Sicily Province during the time period here in focus, but the oldest known deposits date back to *c.* 500 ka (Peccerillo & Frezzotti 2015) and 320 ka (Mahood & Hildreth 1986), respectively. Mount Vulture was dormant between *c.* 160 and 490 ka according to proximal and distal archives (Villa & Buettner 2009).

Material and methods

F4–F5 record

Two parallel cores were obtained from the F4–F5 drill site (42°00'06.22"N, 13°32'17.79"E), which is located close to the centre of the Fucino Basin (Fig. 1A). Seismic information (Cavinato *et al.* 2002) and sedimentation rate estimations based on adjacent previous drilling campaigns (Fig. 1B; GeoLazio, SP cores, F1–F3; Giaccio *et al.* 2015b, 2017a; Mannella *et al.* 2019) suggested this drill site as ideal for reaching older sediments in relatively shallow depth. The 1.5-m-long core segments from the two boreholes were correlated based on core images, X-ray fluorescence (XRF) data and palaeomagnetic information to the 98.11-m-long composite section F4–F5 (Giaccio *et al.* 2019). Grey-whitish lacustrine calcareous marls dominate the sediments and alternate with darkish clay lacustrine muds. Tephra layers are frequently intercalated. The variability of the calcareous content in the F4–F5 sediments is mainly related to variations in the lake's primary productivity and precipitation of endogenic calcite, which depend on temperature and hydrology and thus on glacial–interglacial and sub-orbital climatic variability (Mannella *et al.* 2019).

The uppermost ~35 m of the F4–F5 record were successfully correlated with the tephrostratigraphical framework of the F1–F3 record (Giaccio *et al.* 2019) that

spans the last 190 ka (Giaccio *et al.* 2017a). ⁴⁰Ar/³⁹Ar dating of a tephra layer (TF-126) from the bottom of the F4–F5 succession revealed that the entire record covers the last 425 ka (MIS 12, Giaccio *et al.* 2019). Detailed investigations of the intervals 80.52–98.11 and 31.74–49.02 m correlated depth (m c.d.) presented a comprehensive tephrostratigraphical framework spanning the MIS 11/12 transition until the beginning of MIS 10 (366–425 ka; Monaco *et al.* 2021) and the late MIS 8 to early MIS 6 (*c.* 170–250 ka, Monaco *et al.* 2022b). The focus of the present study is the succeeding interval 60.42–80.52 m c.d., covering the time interval 313–366 ka (MIS 9–10).

XRF core scanning

Individual core halves of the F4–F5 record were scanned using an Itrax XRF scanner (Cox Analytical Systems, Sweden) at the Institute of Geology and Mineralogy of the University of Cologne, Germany. XRF scans were made as described in Giaccio *et al.* (2019) using a Chromium tube set at 55 kV and 30 mA with a dwell time of 10 s and a step size of 2.5 mm.

Tephra identification and sample preparation of F4–F5 tephra layers

Tephra layers were identified during visual core description and subsequent inspection of high-resolution line-scan images. Tephra layers were sampled over their entire thickness as a bulk sample or across subunits, if recognized (e.g. based on colour or clast morphology and grain-size change, cf. Table 1). Tephra layers of <0.5 cm thickness or mixed with larger amounts of lake sediments were prepared following the preparation protocol described in Leicher *et al.* (2021) using HCl for carbonate removal, sieving and heavy liquid separation. If samples were pre-treated, respective information of the analysed fraction is given along with the geochemical data at the EarthChem repository (Leicher *et al.* 2022).

Sampling of proximal equivalents

The Magliano Romano Plinian Fall was resampled north of the Sacrofano caldera of the Sabatini Volcanic District. Sample SAB-01rs corresponds to sample SAB-01 described in Sottili *et al.* (2010). At the Roccamonfina volcano, three subsamples of Unit E and two subsamples of Unit D of the WTT were collected in the same type localities as described by Giannetti & De Casa (2000). Details on section locations and sampled subunits are provided in Table 2.

EPMA-WDS

Major and minor elements of individual glass fragments were analysed by electron microprobe wavelength dis-

Table 1. Tephra layers identified in the time interval 313–366 ka of the F4–F5 succession and information about their position within the record, appearance, lithology and rock composition according to the total alkali vs. silica (TAS) diagram (Le Bas et al. 1986), assignment of compositional group (CG) and their modelled and $^{40}\text{Ar}/^{39}\text{Ar}$ ages. † $^{40}\text{Ar}/^{39}\text{Ar}$ ages of this study; ‡ $^{40}\text{Ar}/^{39}\text{Ar}$ age from Monaco et al. (2021); sa, sanidine; lc, leucite; am, amphibole; cpx, clinopyroxene; bmca, black mica.

Label	Core section and depth (cm)	Bottom depth (m c.d.)	Distance to tephra above (m)	Appearance	Juvenile clasts	Minerals	Rock type (TAS)	CG	Modelled age and $^{40}\text{Ar}/^{39}\text{Ar}$ age (ka)
TF-62 top/middle/bottom	F4 – 39.90.00–94.20–97.60–100.50	60.61	—	Layer	Greyish dark vesicular scoria + brownish and transparent glass shards and micropumice + whitish and greyish pumice	sa, cpx, am	Top = phonolite + tephriphonolite; middle = phonolite + tephriphonolite; bottom = phonolite + tephrite–phonotephrite	1A	314.1±2.4 313.5±1.4†
TF-63	F5 – 39.52.00–53.00	60.95	0.35	Lenses	Black–grey scoria	sa, cpx	Tephrite–phonotephrite–tephriphonolite–phonolite + phonolite–trachyte	3 (1B + 2)	315.3±2.8
TF-64	F4 – 39.113.50–115.00	61.17	0.22	Layer	Grey pumice	lc, sa, cpx, am	Phonolite–trachyte	2	316.0±2.9
TF-64a	F4 – 39.117.50–120.00	61.22	0.05	Layer	White–grey pumice	lc, sa, cpx, bmca	Phonolite–trachyte	2	316.2±2.9
TF-64b	F4 – 40.16.35–17.64	61.97	0.75	Layer	Transparent shards + white micropumice	lc, sa, cpx	Phonotephrite–tephriphonolite–phonolite	1A	318.8±3.2
TF-65	F4 – 40.76.08–77.39	62.56	0.60	Layer	Brown glass, grey scoria	sa, cpx	Tephrite–foidite + K–foidite	1B	320.8±3.3
TF-65a	F4 – 41.39.07–44.62	63.96	1.40	Lenses	Transparent, white and ochre micropumice, grey scoria	sa	Foidite–phonotephrite + phonolite–trachyandesite–trachyte	3 (1A + 1B)	325.3±3.1
TF-66	F4 – 41.105.21–107.64	64.59	0.63	Layer	Brown scoria	sa	Phonotephrite–>> tephriphonolite	1C	327.5±3.0
TF-67	F4 – 41.135.50–136.36	64.88	0.29	Layer	Brown scoria	sa, cpx, lc	Phono–tephrite–tephri–phonolite	1C	328.5±2.8
TF-68 top/bottom	F5 – 41.104.6–106.0–109.0	65.19	0.31	Layer	Top: white ochre micropumice; bottom: transparent, white and few grey micropumice	bmca, sa	Top = phonolite–trachyte (tephriphonolite) + bottom = phonolite – trachyte	1A	329.5±2.6 329.2±3.4†
TF-69 top/bottom	F4 – 42.39.5–49.5 + 49.5–59.80	65.98	0.79	Layer	Top: grey–black scoria, few grey micropumice; bottom: white–transparent micropumice, grey scoria	Top: lc, <sa, bmca; bottom: bmca, sa	Top = (tephriphonolite)–phonolite + bottom = tephrite–phonotephrite – tephriphonolite–phonolite–trachyte	1A	331.5±2.2 331.9±1.0†
TF-70	F5 – 42.95.75–120.00	67.31	1.33	Lenses	Grey–black scoria, grey–white pumice	bmca, sa, lc, amp, cpx	Trachyte	2	335.7±3.0
TF-71	F4 – 43.113.20–116.64	68.48	1.16	Layer	White and transparent micropumice	bmca, sa	Tephriphonolite–phonolite	1A	338.5±3.3
TF-72	F4 – 44.34.50–36.75	69.47	0.99	Lens	Weathered micropumice	sa, bmca, cpx	Trachyte	2	340.8±3.5
TF-73	F4 – 44.103.33–105.38	70.15	0.69	Lenses	Weathered micropumice	bmca, sa, lc, cpx	–	–	342.4±3.5
TF-74	F5 – 44.83.75–89.44	71.01	0.86	Layer	Weathered white micropumice	sa	–	–	344.3±3.5

(continued)

Table 1. (continued)

Label	Core section and depth (cm)	Bottom depth (m c.d.)	Distance to tephra above (m)	Appearance	Juvenile clasts	Minerals	Rock type (TAS)	CG	Modelled age and $^{40}\text{Ar}/^{39}\text{Ar}$ age (ka)
TF-74a	F4–45 146.69–148.99	72.33	1.31	Layer	Grey scoria	bmca, sa, cpx	Tephrite–phonotephrite	IC	347.4±3.5
TF-74b	F5–45 51.91–52.50	72.41	0.08	Layer	–	cpx, bmca, am, sa	–	–	347.6±3.5
TF-74c	F5–45 59.85–60.55	72.49	0.08	Lenses	Weathered white-grey micropumice	cpx, sa	–	–	347.8±3.6
TF-74d	F5–45 64.59–66.28	72.55	0.06	Lenses	White-ochre and grey micropumice	sa, bmca, cpx	Phonotephrite + trachyandesite	IC	347.9±3.5
TF-74e	F5–45 81.86–82.33	72.71	0.16	Layer	White and grey micropumice	bmca, cpx, lc, sa	Phonolite–trachyte–rhyolite	2	348.3±3.6
TF-75	F4–46 30.25–32.25	73.08	0.37	Layer	Black scoria, grey micropumice	sa, lc, bmca	Tephrite–phonotephrite–tephriphonolite	IC	349.2±3.6
TF-76	F4–46 109.31–110.47	73.86	0.78	Layer	Grey and white micropumice, dark-grey and black scoria	sa, bmca, cpx	Tephrite–phonotephrite + phonolite–trachyte	3 (1B + 1A)	350.9±3.0† 350.9±3.6
TF-77	F5–46 46.00–49.00	74.20	0.34	Lens	Dark grey-black scoria, brown micropumice	lc, cpx	Phonotephrite–tephriphonolite–(phonolite)	IC	351.7±3.6
TF-78	F5–46 111.54–112.88	74.84	0.64	Layer	Grey-black scoria, transparent shards	lc, sa, cpx, bmca	Phonotephrite–tephriphonolite–basaltic–trachyandesite–trachyandesite	IC	353.2±3.6
TF-79	F4–47 77.41–78.42	75.69	0.84	Small Lenses	Transparent glass shards	lc, sa, cpx	Tephriphonolite–phonolite + rhyolite	IC	355.1±3.6
TF-80	F5–47 114.86–117.75	76.95	1.26	Small lenses	Weathered micropumice	lc, sa, bmca, cpx	–	–	358.0±3.5
TF-81	F4–49 98.99–103.75	79.83	2.88	Layer	Grey-black scoria, light-grey micropumice	cpx, sa, bmca	Foidite–tephrite + phonolite	3 (1B + 1A)	364.5±3.0
TF-82	F4–49 122.50–125.05	80.05	0.21	Layer	Grey pumice, black scoria	cpx, sa, bmca	Foidite–tephrite –phonotephrite + phonolite	3 (1B + 1A)	362.7±5.0† 365.0±3.0
TF-83	F4–49 134.57–135.16	80.15	0.10	Lenses	Grey, dark-grey scoria	cpx, sa, bmca	Foidite + tephrite	IB	365.3±3.0
TF-84	F5–49 57.75–58.17	80.23	0.08	Layer	Grey, dark-grey scoria	sa, lc, cpx, bmca	Tephrite–phonotephrite–balsaltic trachyandesite/shoshonitic	IB	365.5±2.9
TF-85	F5–49 74.25–87.50	80.52	0.29	Layer	Darkish black porphyritic lc-bearing scoria and aphyric highly vesicular black scoria	lc, bmca, lithics	Foidite–phonolite	ND	365.9±2.9 365.8±1.4‡

Table 2. Locations for the samples from the Roccamonfina lower White Trachytic Tuff (WTT) and the Magliano Romano Plinian Fall (MRPF) of the Sabatini volcanic district investigated in this study. The lower WTT sample sites were revisited from Giannetti & De Casa (2000) and for the MRPF from Sottili *et al.* (2010).

Site coordinates (deg.)				Sample	Unit	Subunit
Site	Site literature	Lat.	Long.			
WTT						
RCM5	88	41.260	13.908	RCM-05	WTT E	E 2
RCM6	88	41.260	13.908	RCM-06		E 1–2
RCM1	56	41.261	13.913	Base UE		E Base
				RCM-02	WTT D	D-Flow
				RCM-01		MKDP
MRPF						
MRPF	SAB-01	42.141	12.422	SAB-01rs	Main eruptive phase	Whitish pumice

persive spectroscopy (EPMA-WDS) for determining the geochemical fingerprint of the respective tephra layer. Samples were measured at the Istituto di Geologia Ambientale e Geoingegneria of the Italian National Research Council (IGAG-CNR, Rome, Italy) and the University of Cologne (Germany). Analyses at IGAG-CNR were performed with a Cameca SX50 electron microprobe equipped with five-wavelength dispersive spectrometers and operated with an accelerating voltage of 15 kV, a beam current of 15 nA, a beam diameter of 10 μm and a counting time of 20 s per element (full details of calibration and measuring conditions are given in Leicher & Giaccio 2021). A Jeol JXA-8900RL electron microprobe equipped with five-wavelength dispersive spectrometers was used for analyses at the University of Cologne. The operation conditions were set to 12 kV accelerating voltage, 6 nA beam current and 5 μm beam diameter. Full details of calibration and measuring conditions are given in Leicher (2021). Information on which laboratory the respective sample was measured in is given along with individual geochemical data at the EarthChem repository (Leicher *et al.* 2022). Analytical differences caused by the different EPMA-WDS settings of the IGAG-CNR and University of Cologne laboratories are discussed in detail in Leicher *et al.* (2021). In general, IGAG-CNR results are higher for SiO_2 and MgO and lower for FeO , Mn , Na_2O relative to those obtained at the University of Cologne, whereas concentrations of TiO_2 , Al_2O_3 , CaO and Cl do not show systematic deviations. Only EPMA-WDS geochemical analyses of glass fragments with analytical totals >90 wt % were considered and normalized to 100% on a loss on ignition free basis, excluding volatiles (Cl , SO_3 and F).

⁴⁰Ar/³⁹Ar dating

Six tephra layers (TF-82/-81/-75/-69/-68/-62; Table 1) were selected and subsequently sieved using mesh sizes of 500, 350 and 250 μm . Except for sample TF-62,

the 500–350 and 350–250 μm fractions were further separated using a FRANTZ magnetic separator at the University of Cologne. The respective non-magnetic fractions at 1.5 A and aliquots of TF-62 were washed with distilled water, before transparent, inclusion-free sanidine and/or leucite crystals were handpicked under a binocular microscope and sent to the Laboratoire des Sciences du Climat et de l'Environnement (LSCE, CEA, CNRS UMR 8212, Gif-sur-Yvette, France). At the LSCE facility, crystal aliquots underwent an additional purity screening and were selected based on available crystal sizes (500–350 μm fraction for TF-62/-68/-69/-75 and 350–250 μm fraction for TF-81/-82). Between 20 and 30 crystals of each tephra layer were irradiated for 120 min in the Cd-lined, in-core CLICIT facility of the Oregon State University TRIGA reactor (IRR, CO-007 for TF-62, TF-68, TF-69 and CO-008 for TF-75, TF-81 and TF-82). Interference corrections were based on the nucleogenic production ratios given in Balbas *et al.* (2016). After irradiation, individual crystals of each tephra layer were transferred into a copper 133 pits sample holder placed in a differential vacuum Teledyne Cetac window connected to a home-designed compact extraction line. Individual minerals were fused using a 100 W Teledyne Cetac CO_2 laser during 15 s at a power of 2.5 W. Before fusion, each crystal underwent a 10-s-long sweeping at 0.3 W to remove potentially trapped unwanted gas on the crystals surface and fractures. Extracted gases were firstly purified by a SAES GP 50 cold Getter for 90 s and then for 230 s by two hot SAES GP 50 Getters. Argon isotopes (i.e. ⁴⁰Ar, ³⁹Ar, ³⁸Ar, ³⁷Ar and ³⁶Ar) were measured using a multicollector NGX 600 mass spectrometer equipped with a nine ATONA® amplifier array and an electron multiplier. More technical specifications regarding the NGX 600 ATONA detector array are presented in Cox *et al.* (2020). ⁴⁰Ar, ³⁹Ar and ³⁸Ar isotopes were measured simultaneously using three ATONA® amplifiers together with an electron multiplier for ³⁶Ar isotopes, which was also used for ³⁷Ar in a second run. Each isotope measurement corresponds to 15 cycles of 20 s integration time. Peak intensity data were reduced using ArArCALC V2.4 (Koppers 2002). The neutron fluence J factor was calculated using co-irradiated Alder Creek sanidine (ACs) standard ACs-2 associated with an age of 1.1891 Ma (Niespolo *et al.* 2017) according to the K total decay constant of Renne *et al.* (2011) ($\lambda_{\text{ec}} = (0.5757 \pm 0.016) \times 10^{-10} \text{ a}^{-1}$ and $\lambda_{\beta^-} = (4.9548 \pm 0.013) \times 10^{-10} \text{ a}^{-1}$). To determine the neutron flux for each sample, at least six flux monitor crystals from pits framing the samples in each irradiation disc were used. The J -values are the following: TF-62, $0.00056060 \pm 0.00000045$; TF-68, $0.00056080 \pm 0.00000062$; TF-69TOP, $0.00056060 \pm 0.00000039$; TF-69BOTTOM, $0.00056080 \pm 0.00000056$; TF-75, $0.00055710 \pm 0.00000072$; TF-81, $0.00055750 \pm 0.00000061$; and TF-82, $0.00055800 \pm 0.00000084$. To ensure the detector linearity, mass discrimination was daily monitored by analysis of at least 15 air shots of

various beam sizes ranging from 5.0×10^{-3} to 2.0×10^{-2} V (one to four air shots) automatically generated during the nights before and after the unknown measurements. Discrimination was calculated according to the $^{40}\text{Ar}/^{36}\text{Ar}$ ratio of 298.56 (Lee *et al.* 2006). Procedural blank measurements were achieved after every three unknowns. For a typical 5 min time blank backgrounds are between 2.1 and 3.2×10^{-4} V for ^{40}Ar and 60–90 cps for ^{36}Ar (about 1.0 – 1.3×10^{-6} V equivalent). Full analytical data for each sample can be found in Table S1.

Age–depth modelling

Age–depth modelling was performed using the software package Bacon v. 2.5.7 (Blaauw & Christen 2011) within the open-source statistical environment R (Team 2022). It was based on $^{40}\text{Ar}/^{39}\text{Ar}$ ages of tephra layers identified within the sediment succession between 60.52 and 80.52 m c.d. (Fig. 2). The entire succession was divided into 10 cm vertical sections for modelling individual accumulation rates at a 99% confidence interval, which provide the basis for the age–depth model. Major sedimentological changes identified during core description and within the XRF-downcore data were considered via the ‘boundary’ function within the model. The resulting succession and subsequent profile depth were adjusted for tephra layers with a thickness of more than 5 cm to avoid bias of accumulation rates by these rapid depositional events. An individual age was calculated for each tephra layer.

Results

Sediment lithology and texture and geochemical composition of tephra layers

The sediment between 60.42 and 80.52 m c.d. can be split into two main lithological units. The lower unit (67.50–80.52 m c.d.) consists of carbonate-poor, greenish-bluish silty clays, whereas carbonate-rich, brownish-ochre clayey silts characterize the upper unit (60.42–67.50 m c.d.). Within the upper unit, no sediments were recovered between 63.32 and 63.66 m c.d. The interval 66.6–67.5 m c.d. marks a transition between the two units. Overall, 32 horizons containing volcanic fragments (e.g. juvenile glass fragments and/or pyrogenic minerals) were identified. The position of these tephra horizons and their characteristic lithological features, i.e. thickness, colour, morphological appearance, type of juvenile fragments and mineral assemblage, are given in Table 1. Tephra horizons are intercalated in fine-grained lake sediments as massive discrete layers and single or arrays of lenses, and vary in thickness between 0.4 and 24.3 cm. Bioturbation, sediment load and/or drilling disturbance structures are present, but had only a minor effect on the preservation of most of the tephra layers (e.g. for determining the position of the isochrone or

internal structures). Tephra layers TF-65a/-70/-72, were affected by drilling-induced disturbances (centimetre-scale displacement).

Of the 32 identified layers, 25 tephra layers contained sufficient amounts of well preserved and unaltered glass fragments suitable for EPMA-WDS analyses. Two of these tephra (TF-62/-85) were analysed in previous studies (Giaccio *et al.* 2019; Monaco *et al.* 2021), of which TF-62 is re-examined here. Among the seven other tephra, tephra layers TF-72/-74d contained only one and three fresh glass shards, respectively. The other five tephra layers (TF-73/-74/-74b/-74c/-80) contained exclusively minerals and/or heavily weathered glass fragments, and thus were not suitable for the determination of their glass geochemical fingerprints.

The full dataset of EPMA-WDS analyses is available at the EarthChem repository (Leicher *et al.* 2022). The individual classification of tephra layers according to the total alkali vs. silica (TAS) diagram after Le Bas *et al.* (1986) is summarized in Table 1 and visualized in Fig. 3. Tephra layers show most of the compositional features typical for volcanic rocks known from peri-Tyrrhenian volcanoes including tephrites, phonotephrites, tephri-phonolites, phonolites, foidites, trachytes and rhyolites. Based on their compositional differences, the newly investigated tephra layers from Fucino can be split into three compositional groups (Table 1, Fig. 3): CG1 (tephrite–phonolites, $n = 16$), CG2 (phonolite–trachyte–rhyolites, $n = 5$) and CG3 (tephrite–phonotephrites and phonolite–trachytes, $n = 5$). The definition of the compositional groups is given along with the discussion about the volcanic origin of tephra layers below.

$^{40}\text{Ar}/^{39}\text{Ar}$ chronology

The results of $^{40}\text{Ar}/^{39}\text{Ar}$ dating of individual tephra layers are presented as probability diagrams (Fig. 2). Weighted mean age uncertainties are reported at 2σ , including J uncertainty, and were calculated using Isoplot 4.1 (Ludwig 2009). Inverse isochrones of individual samples are characterized within uncertainties by an atmospheric $^{40}\text{Ar}/^{36}\text{Ar}$ initial intercept, suggesting that dated crystals are without detectable excess argon.

TF-62. – 15 sanidine crystals were individually dated for this layer. The probability diagram (Fig. 2A) is multimodal with four clearly older crystals ranging from about 327.5 to 437.9 ka. The youngest population, including the majority of the sanidines (11 crystals), is interpreted as juvenile and provides a weighted mean age of 313.5 ± 1.4 ka (Mean Squared Weighted Deviation (MSWD) = 0.47, $p = 0.92$).

TF-68. – Fourteen individual crystals (nine sanidine and five leucite) were dated. Excluding one older crystal with

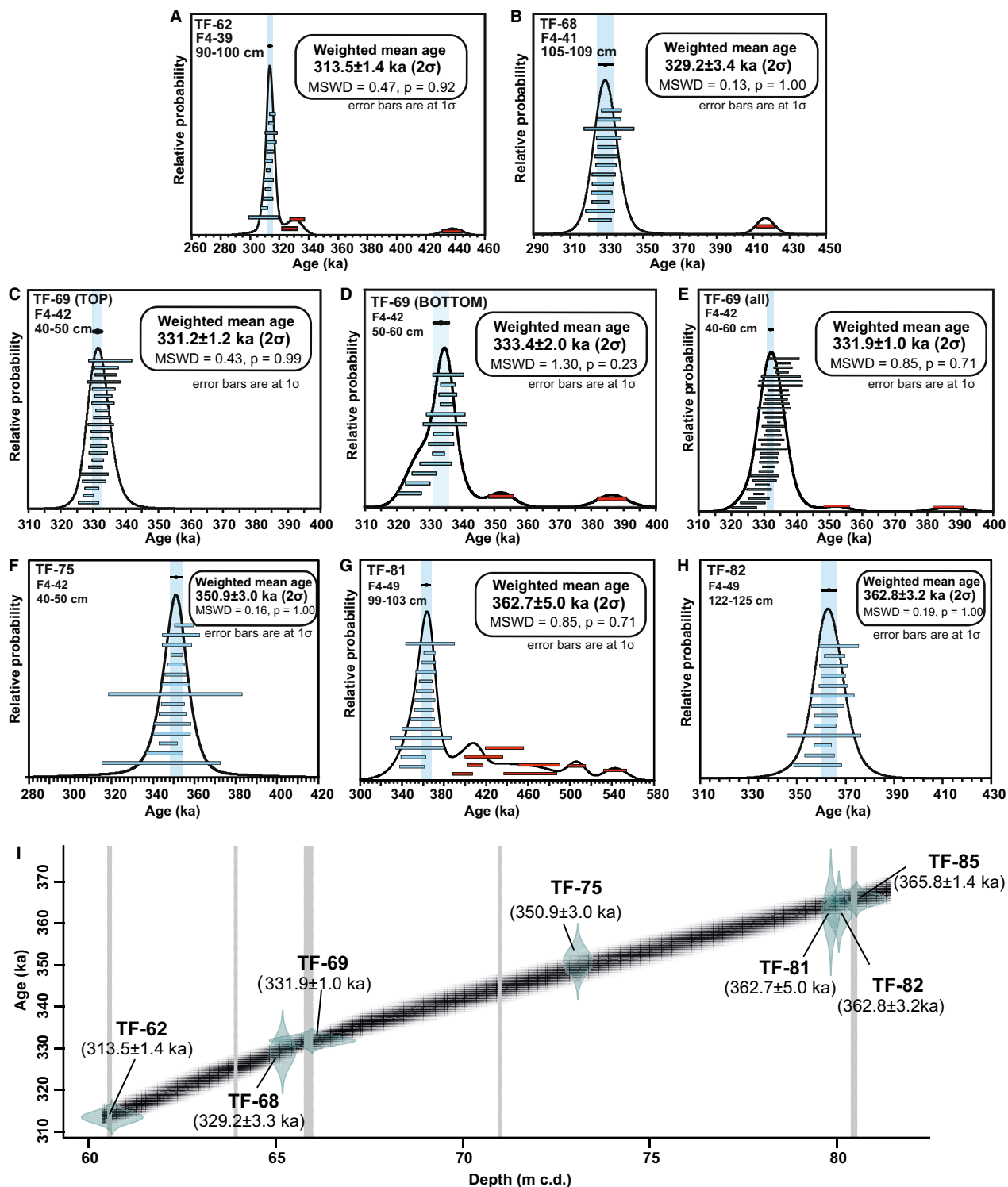
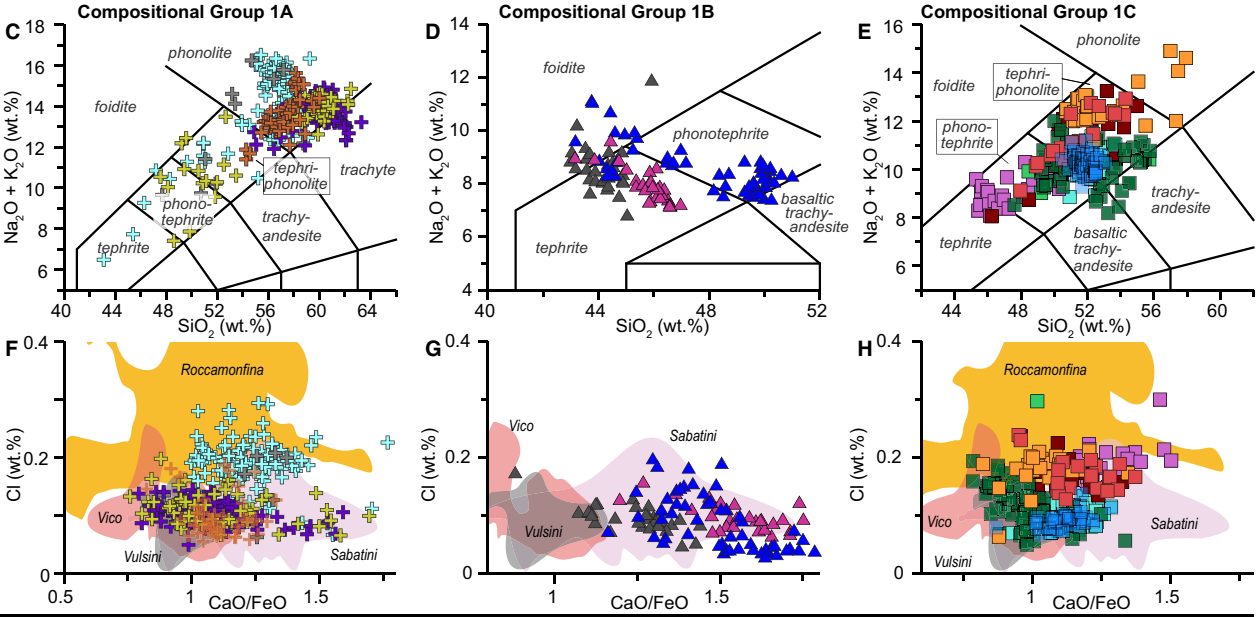
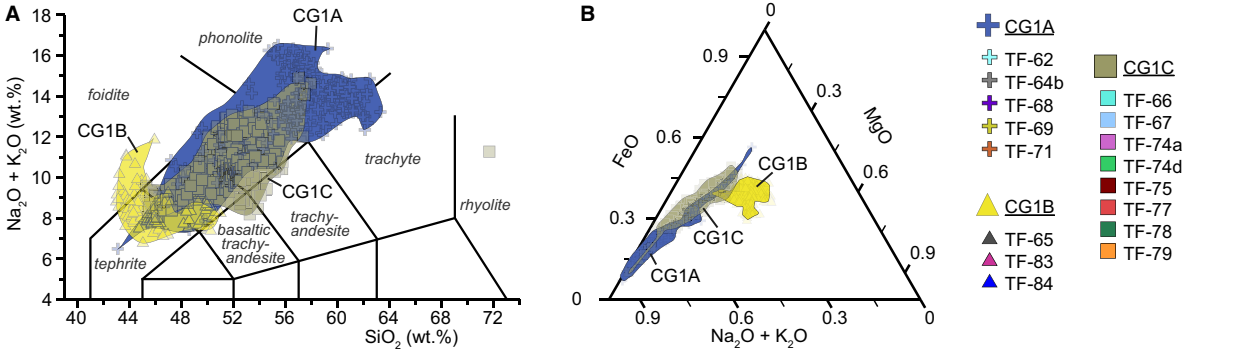


Fig. 2. A–H. Relative probability diagrams of single crystal fusion $^{40}\text{Ar}/^{39}\text{Ar}$ ages of tephra layers TF-62, TF-68, TF-69 (top, bottom, combined), TF-75, TF-81, TF-82. I. Age–depth model based on available $^{40}\text{Ar}/^{39}\text{Ar}$ ages of tephra layers of the studied interval. Grey bars illustrate tephra layers with thickness ≥ 5 cm and for which the succession depth was corrected.

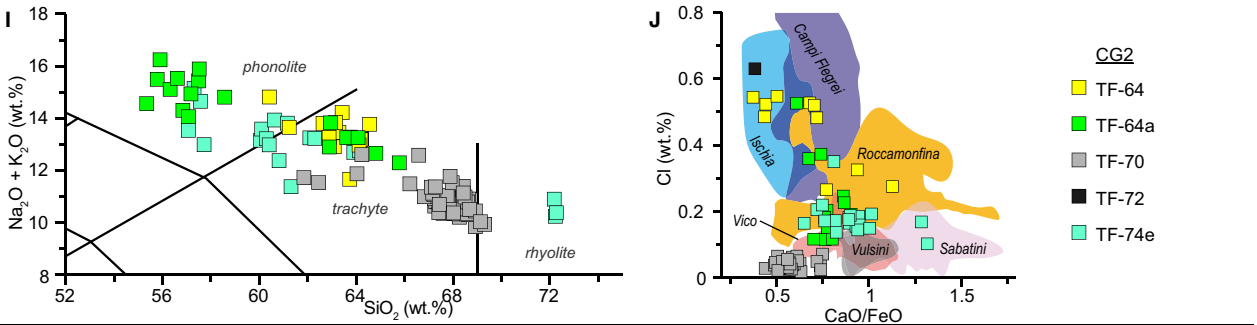
an age of 416.8 ka, a main population constituted by 13 crystals (Fig. 2B) allows the calculation of a weighted mean age of 329.2 ± 3.4 ka (MSWD = 0.13, $p = 1.00$).

TF-69. – TF-69 was split based on visual differences into two distinct subunits (Table 1), which were treated and dated separately. A total of 15 crystals were dated for

Compositional Group 1



Compositional Group 2



Compositional Group 3

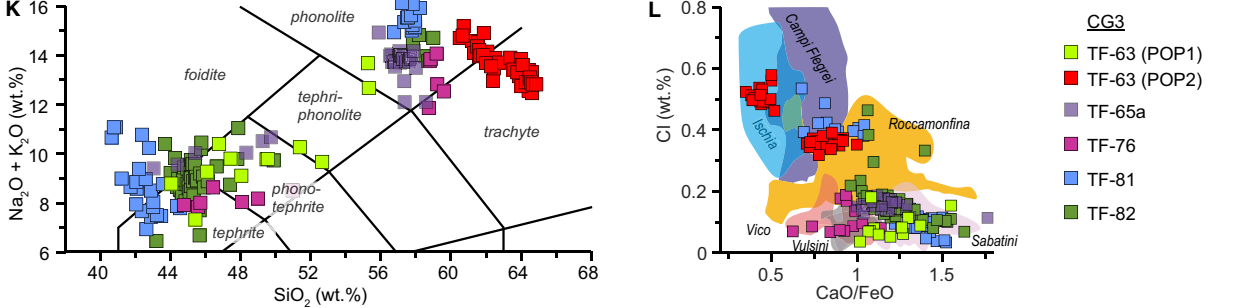


Fig. 3. Geochemical classification and overview of compositional groups CG1-3. Alkali vs. silica (TAS) classification according to Le Bas et al. (1986). CaO/FeO vs. Cl diagram shows the different volcanic origins based on Giaccio et al. (2017a).

subunit TF-69BOTTOM. The Ca/K ratios of the analysed crystals demonstrate that this subunit mainly comprises sanidines (12 crystals) and only a small proportion of leucites (three crystals). The related probability diagram (Fig. 2C) displays two obviously older crystals (352 ± 8 and 387 ± 9 ka). The main mode that is interpreted as juvenile crystals (13 crystals) provides a weighted mean age of 333.4 ± 2.0 ka (MSWD = 1.30, $p = 0.23$). For subunit TF-69TOP, 21 crystals (19 leucites and two sanidines according to the Ca/K ratios) were dated and provided the same age within uncertainties, thus allowing calculation of a precise weighted mean age of 331.2 ± 1.2 ka (Fig. 2D, MSWD = 0.43, $p = 0.99$). Within uncertainties the two units are chronologically indistinguishable and enable the calculation of a combined weighted mean age of 331.9 ± 1.0 ka (Fig. 2E, MSWD = 0.85, $p = 0.71$).

TF-75. – Fifteen leucite crystals were individually dated. Owing to the small size of the crystals ($< 350 \mu\text{m}$), individually calculated ages are less precise than for other tephra layers. However, all crystals analysed gave within uncertainty the same age, resulting in a Gaussian probability diagram (Fig. 2F). Based on this very homogeneous crystal population, a weighted mean age of 350.9 ± 3.0 ka (MSWD = 0.16, $p = 1.00$) was calculated.

TF-81. – Twenty-two leucite crystals were dated individually for this tephra layer. Despite the relative low precision of the individual ages that can be explained by the small size of the crystals, several distinct crystal populations can be distinguished. A clear contamination (8/22 dated crystals) ranging between 390 and 543 ka is demonstrated by the probability diagram (Fig. 2G). The youngest homogeneous population constitutes 14 crystals and was used to calculate a weighted mean age of 362.7 ± 5.0 ka (MSWD = 0.85, $p = 0.71$).

TF-82. – For this layer 13 single leucite crystal ages were obtained. All of them are undistinguishable within uncertainty, resulting in a single mode probability diagram (Fig. 2H). This homogeneous population of crystals allows the calculation of a robust weighted mean age of 362.8 ± 3.2 ka (MSWD = 0.19, $p = 1.00$) for this tephra layer.

Age–depth modelling

The six new $^{40}\text{Ar}/^{39}\text{Ar}$ ages and the previously obtained age of TF-85 (365.8 ± 1.4 ka, Monaco et al. 2021) provided the basis for age–depth modelling, with TF-62

framing the model at the top and TF-85 at the bottom. The lithological change identified during the core description (colour, grain size, carbonate content) and in XRF downcore data (elements related to carbonate content, clastic input) at about 67.5 m c.d. marks the transition from glacial to interglacial conditions (Giaccio et al. 2019; Mannella et al. 2019). This change was considered in the age model by setting a boundary function, accounting for different sedimentation rates during glacial and interglacial conditions. Overall, the age–depth model (Fig. 2I) suggests continuous sedimentation with a mean accumulation rate of 24.6 a cm^{-1} (40.5 cm ka^{-1}) during the glacial MIS 10 and 31.2 a cm^{-1} (27.8 cm ka^{-1}) during the interglacial MIS 9. Based on the age–depth model, an age with a 2σ uncertainty could be assigned to each undated tephra layer (Table 1). For the discussion on the volcanic origin and potential individual correlations of tephra layers, all $^{40}\text{Ar}/^{39}\text{Ar}$ ages from literature discussed in the text (Table 3) were recalculated to ACs at 1.1891 Ma (Niespolo et al. 2017) using the decay constant of Renne et al. (2011).

Volcanic origin of tephra layers

General compositional features and temporal span of investigated tephra layers

Homogeneous compositions or continuous compositional trends are observed for most (20/27) of the analysed tephra layers and indicate individual volcanic sources and events (Fig. 3). However, seven tephra layers have a heterogeneous composition with distinct geochemical populations. Tephra layers of CG3 (TF-63/65a/76/81/82) show a bimodal composition, with a primitive tephritic–phonotephritic and a more evolved phonolitic–trachytic population, which are separated by a silica gap (populations with mean-SiO₂ of 46 and 60 wt%, respectively). The bimodal composition can be interpreted as compositional gap of a single event or by mixing of different eruptions in one layer. However, for TF-65a, TF-76, TF-81 and TF-82 a reworked origin and thus a mix of different eruptions appears unlikely. Their specific compositions do not reflect those of the adjacent tephra layers, nor do they show a more heterogeneous mix of several eruptions ($n > 2$), which would be expected for reworked tephra (e.g. wash-in of several different tephra deposited from the catchment). Furthermore, their individual compositions follow the same magmatic evolutionary trend. This trend is not seen in the composition of TF-63, which may represent two different volcanic origins. The other multicompositional tephra

Table 3. Summary of available $^{40}\text{Ar}/^{39}\text{Ar}$ ages discussed in the text and in Fig. 8. For a homogenized comparison, all ages were recalculated to ACs at 1.1891 Ma (Niespolo *et al.* 2017) and the decay constant of Renne *et al.* (2011). Uncertainties are given at a 2σ level including analytical and J -value uncertainties. BLT = Brown Leucitic Tuff.

Volcanic source	Eruptive event/name of tephra	Original age (ka)	Recalculated age (ka)	Reference
Undefined Roman origin	Capitoline Hill (CH-AF)	352.2±1.7	350.8±1.7	Marra <i>et al.</i> (2016a)
Roccamonfina	LWTT Unit E	301.0±2.0	306.7±5.0	Giannetti & De Casa (2000)
Roccamonfina	LWTT Unit E1	305.0±30.0	309.9±30.0	Giannetti & De Casa (2000)
Roccamonfina	LWTT (MOL10/14)	311.0±5.0	312.1±5.0	Amato <i>et al.</i> (2014)
Roccamonfina	LWTT Unit D	308.0±4.0	312.9±4.0	Giannetti & De Casa (2000)
Roccamonfina	LWTT Unit C	312.0±8.0	317.0±8.0	Giannetti & De Casa (2000)
Roccamonfina	LWTT Unit B	314.0±10.0	319.0±10.0	Giannetti & De Casa (2000)
Roccamonfina	LWTT Unit A	317.0±4.0	322.0±4.0	Giannetti & De Casa (2000)
Roccamonfina	undefined LWTT	331.0±2.0	331.5±2.0	Quidelleur <i>et al.</i> (1997)
Roccamonfina	BLT	344.5±11.2	347.7±11.2	Scaillet <i>et al.</i> (2008)
Roccamonfina	BLT	353.0±5.0	352.0±5.0	Rouchon <i>et al.</i> (2008)
Roccamonfina	Guado San Nicola (SU-Tufi)	345.0±5.2	343.9±5.2	Pereira <i>et al.</i> (2016)
Roccamonfina	BLT (LS7)	349.0±3.0	352.3±3.0	Santello (2010)
Roccamonfina	BLT (LS8)	350.0±3.0	352.4±3.0	Santello (2010)
Roccamonfina	Scipicciano (89X)	356.0±5.0	355.1±5.0	Rouchon <i>et al.</i> (2008)
Roccamonfina	Fontana-Radina (RMF7)	358.0±8.0	357.1±8.0	Rouchon <i>et al.</i> (2008)
Roccamonfina	Galluccio (RMF3)	368.0±9.0	367.1±9.0	Rouchon <i>et al.</i> (2008)
Roccamonfina	La Frascara (RMF4)	370.0±8.0	369.0±8.0	Rouchon <i>et al.</i> (2008)
Sabatini	Tufo Giallo di Sacrofano (SAB-49)	286.0±8.0	288.0±6.0	Sottili <i>et al.</i> (2010)
Sabatini	Tufo di Bracciano (SAB-15)	307.0±5.0	310.0±5.0	Sottili <i>et al.</i> (2010)
Sabatini	Magliano Romano Plinian fall (SAB-01)	310.0±2.0	312.8±2.0	Sottili <i>et al.</i> (2010)
Sabatini	Monte Musino (SAB-52)	316.0±6.0	319.1±6.0	Sottili <i>et al.</i> (2010)
Sabatini	Tufo di Bracciano (SAB-71)	316.0±6.0	319.1±6.0	Sottili <i>et al.</i> (2010)
Sabatini	Monte Rocca Romana (SAB-05)	317.0±14.0	320.1±14.0	Sottili <i>et al.</i> (2010)
Sabatini	Tufo di Bracciano (POL12-01±03)	325.0±2.0	323.9±2.0	Pereira <i>et al.</i> (2017)
Vulsini	WOB	296.0±7.0	306.8±7.0	Turbeville (1992)
Vulsini	Cluster CB-4-5	321.9±0.9	322.3±0.9	Marra <i>et al.</i> (2020b)
Vulsini	CB-2	327.5±3.5	328.2±3.5	Marra <i>et al.</i> (2020b)
Vulsini	CB-260	328.7±1.6	329.4±1.6	Marra <i>et al.</i> (2020b)
Vulsini	Cluster CB-2-3-4-260	330.0±1.0	330.8±1.0	Marra <i>et al.</i> (2020b)
Vulsini	WOB	333.0±3.8	332.2±3.8	Nappi <i>et al.</i> (1995)
Vulsini	CB-3	334.7±1.5	335.5±1.5	Marra <i>et al.</i> (2020b)
Vulsini	Cluster CB-3	337.1±1.2	337.9±1.2	Marra <i>et al.</i> (2020b)
Vulsini	CB-2-4-200-260	345.8±1.4	346.6±1.4	Marra <i>et al.</i> (2020b)
Vulsini	Ponticello Pumices	351.7±4.0	350.9±4.0	Nappi <i>et al.</i> (1995)
Vulsini	TOR1±POL12-02	355.0±4.0	353.5±4.0	Marra <i>et al.</i> (2016a)
Colli Albani	Monte Castellaccio (CAS-01)	351.0±3.0	354.5±3.0	Karner <i>et al.</i> (2001)
Colli Albani	Monte Ferrari (AH39)	357.0±9.0	355.8±9.0	Marra <i>et al.</i> (2003)
Colli Albani	Sincrotrone (S3C1) 1	355.1±9.3	356.3±9.3	Gaeta <i>et al.</i> (2016)
Colli Albani	Nemi (AH4A)	365.0±2.0	363.8±2.0	Marra <i>et al.</i> (2003)
Colli Albani	Tavernole lower (AH35) 2	366.0±3.0	364.8±3.0	Gaeta <i>et al.</i> (2016)
Colli Albani	Pantano Secco (AH11-B1)	364.5±1.2	365.3±1.2	Marra <i>et al.</i> (2016b)
Colli Albani	Villa Senni	365.8±1.4	365.8±1.4	Monaco <i>et al.</i> (2021)
Colli Albani	Valle Marciana (AH10)	367.0±2.0	365.8±2.0	Marra <i>et al.</i> (2003)
Colli Albani	Prata Porci (AH8-F2)	365.3±1.2	366.1±1.2	Marra <i>et al.</i> (2016b)
Volsci Volcanic Field	MOS-2	330.9±2.6	332.1±2.6	Marra <i>et al.</i> (2021a)
Volsci Volcanic Field	PO-C6	337.5±6.4	338.3±6.4	Marra <i>et al.</i> (2021b)
Volsci Volcanic Field	CA-C1	345.4±4.3	347.2±4.3	Marra <i>et al.</i> (2021a)
Volsci Volcanic Field	ERN 20	345.0±7.0	348.3±7.0	Boari <i>et al.</i> (2009b)
Volsci Volcanic Field	GdR-1	349.5±5.0	350.8±5.0	Marra <i>et al.</i> (2021a)
Volsci Volcanic Field	K-layer	353.0±4.0	351.8±4.0	Nomade <i>et al.</i> (2011)
Volsci Volcanic Field	CA-CGT	359.6±6.5	360.1±6.5	Marra <i>et al.</i> (2021a)
Volsci Volcanic Field	ERN 91	359.0±11.0	362.4±11.0	Boari <i>et al.</i> (2009b)
Volsci Volcanic Field	Isoletta ESR 4	365.1±3.8	363.2±3.8	Pereira <i>et al.</i> (2018)
Volsci Volcanic Field	ERN 23	376.0±8.0	379.7±8.0	Boari <i>et al.</i> (2009b)
Volsci Volcanic Field	CE-2	389.6±3.7	391.0±3.7	Marra <i>et al.</i> (2021b)

layers TF-65 and TF-79 show dominant homogeneous populations (10–48 shards) accompanied by a second very minor population (one to three shards). The very

limited number of shards of the minor population and their geochemical composition differing distinctively from the main population suggest displaced material

owing to either natural (e.g. bioturbation, wash in of reworked material) or artificial processes (e.g. drilling, core processing).

The only volcanic sources identified for F4–F5 tephra layers in previous studies were the proximal peri-Tyrrhenian volcanoes (Giaccio *et al.* 2017a, 2019; Del Carlo *et al.* 2020; Monaco *et al.* 2021, 2022b). Also the spectrum of geochemical compositions analysed within the interval 313–366 ka from the F4–F5 record overlaps with those of the Roman, the Roccamonfina and the Campanian Provinces (Provinces after Peccerillo & Frezzotti (2015), see also Fig. 3) and thus confirms a peri-Tyrrhenian origin. Previous tephrochronological studies of the F4–F5 record and the new $^{40}\text{Ar}/^{39}\text{Ar}$ ages provide a chronostratigraphic framework for the investigated interval. TF-85 and TF-62 set the chronological boundaries of the investigated interval. Tephra TF-85 from the bottom of the investigated interval was correlated with the Villa Senni eruption from Colli Albani (Giaccio *et al.* 2019) and precisely $^{40}\text{Ar}/^{39}\text{Ar}$ dated at 365.8 ± 1.4 ka (Monaco *et al.* 2021). Tephra TF-62 from the top of the interval was previously correlated with the Tufo Giallo di Sacrofano (TGDS; 288.0 ± 6.0 ka; Sottili *et al.* 2010; Giaccio *et al.* 2019). However, direct $^{40}\text{Ar}/^{39}\text{Ar}$ dating of the layer provides a significantly older age of 313.5 ± 1.4 ka, questioning a possible correlation with the TGDS. The chronological boundaries of the investigated interval set by TF-85 and TF-62 narrow the number of possible equivalents for individual correlations.

Compositional group 1 (CG1)

Tephra layers of CG1 are characterized by a composition evolving from tephrites to phonolites or trachytes and represent the majority (16/27) of tephra layers analysed within this study. CG1 tephra layers plot within the overlapping TAS fields of known compositions from the Campanian, the Roman, and Roccamonfina and Volsci volcanoes (Fig. 3A). According to the CaO/FeO vs. Cl diagram (Fig. 3F–H) CG1 compositions plot within the fields of Roccamonfina and, more pronounced, volcanoes of the Roman Province, while an origin from the Campania-Neapolitan volcanoes can be ruled out. Owing to the wide compositional spectrum of CG1 tephra layers, the group can be subdivided into three subunits (CG1A, -1B, -1C) based on their different degree in magmatic evolution (cf. Fig. 3A, B dominant rock classification in the TAS and alkali–FeO–MgO diagram).

Compositional group 1A (CG1A). – TF-62/64b/68/69/71 form the sub-compositional group CG1A, which encompasses the most evolved compositions of CG1. The majority of analysed shards have phonolitic and/or trachytic compositions with only minor portions of less evolved products being classified as tephriphonolitic,

phonotephritic or tephritic (TF-62 only). All tephra layers have alkali ratios ($\text{K}_2\text{O}/\text{Na}_2\text{O}$) > 1, reaching high values of 1.5–2.6 for the dominant phonolitic and trachytic populations. Regarding their CaO/FeO ratios (mean = 1.1–1.3) and characteristic low Cl contents (mean = 0.1–0.2 wt%), tephra layers are similar to known compositions of eruptions from the Roman Province, of which only the SVD and the VVD were active during the time window explored here.

TF-62 ($^{40}\text{Ar}/^{39}\text{Ar}$ age 313.5 ± 1.4 ka). – Tephra layer TF-62 has a threefold lithological zonation (top, middle and bottom subunits; Table 1), that is dominated by a phonolitic composition. In addition, some less evolved tephritic components were identified in the bottom subunit and some tephriphonolitic shards were found in the middle and top subunits. The phonolitic composition slightly differs from that of the other CG1A tephra layers by higher Al_2O_3 , Na_2O and Cl values, whereas TiO_2 , FeO, MnO, MgO and CaO are at the given SiO_2 value lower compared with other CG1A compositions. Within the CaO/FeO vs. Cl diagram, the composition overlaps with both the SVD and Roccamonfina fields (Fig. 3F). The new $^{40}\text{Ar}/^{39}\text{Ar}$ age of 313.5 ± 1.4 ka directly obtained on TF-62 questions the former correlation with the Tufo Giallo di Sacrofano eruption (TGDS; 288.0 ± 6.0 ka; Sottili *et al.* 2010; Giaccio *et al.* 2019). The Magliano Romano Plinian Fall (MRPF) is a slightly older eruptive event of the Sacrofano area of the SVD and matches with its age of 312.8 ± 2.0 ka (Sottili *et al.* 2010) that of TF-62. Also the lithological zonation of the MRPF is similar to that of TF-62, with a basal black scoria subunit, topped by the main whitish, well vesicular, leucite-bearing tube pumice lapilli, and an upper subunit of dark grey, moderately vesicular, leucite-bearing pumice lapilli (Sottili *et al.* 2010). The new obtained geochemical data of the MRPF further support the correlation with TF-62, as they are representative of the main unit displaying the most evolved phonolitic compositions (Figs 4A–C, S1A, B). It is likely that the less evolved compositions observed for TF-62 refers to the black scoria MRPF subunit as described in proximal settings by Sottili *et al.* (2010). However, this subunit was not analysed within this study.

TF-64b (modelled 318.8 ± 3.2 ka). – Tephra TF-64b has a phonotephritic–tephriphonolitic–phonolitic composition (mean $\text{K}_2\text{O}/\text{Na}_2\text{O} = 2.0$), which indicates, according to the CaO/FeO vs. Cl diagram, an origin in the SVD field (Fig. 3F). Volcanic activity of similar age within the SVD is known from the Bracciano caldera with the Tufo di Bracciano eruptive phase, which represents the main caldera forming event (Sottili *et al.* 2010). The age of the eruption is imprecisely constrained in proximal settings between 310.0 ± 5.0 and 319.1 ± 6.0 ka. (Sottili *et al.* 2010), whereas associated equivalent volcanic deposits found in the archaeological site of La Polledrara

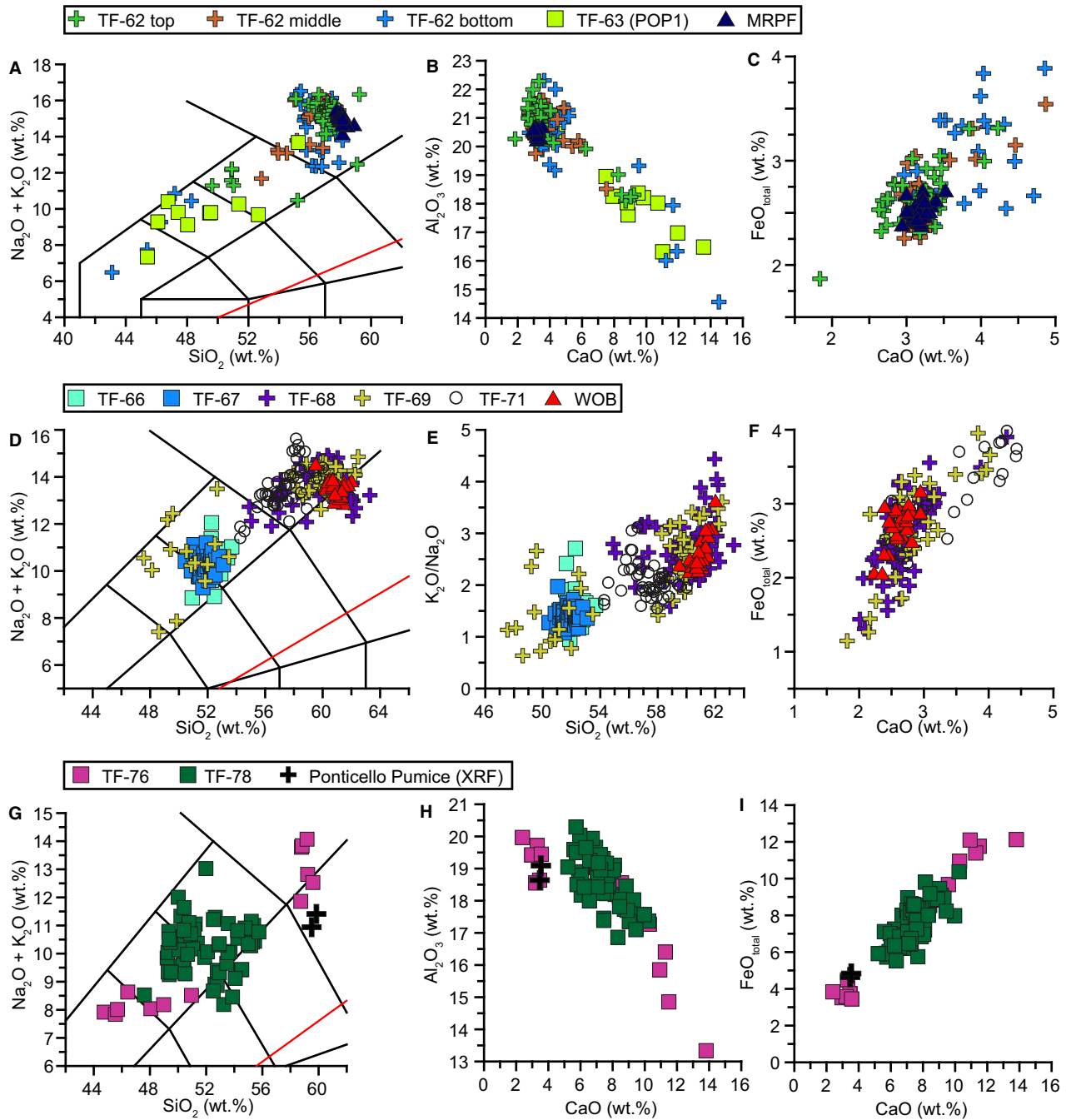


Fig. 4. TAS diagram and bi-variate plots of tephra layers associated with the SVD and VVD. A–C: Comparison of TF-62, TF-63 and the MRPF. In plot (C) only shard compositions for <5 wt% CaO were plotted. D–F: Comparison of TF-66/67/68/69/71 and the WOB eruption with data from Palladino *et al.* (2014). G–I: Comparison of TF-76/78 with X-ray fluorescence (XRF) data of the Ponticello Pumices provided by Nappi *et al.* (1994).

di Ceanibbio suggest an age of 323.9 ± 2.0 ka (Pereira *et al.* 2017). Minor explosive activity of the SVD is also known from Monte Musino (319.1 ± 6.0 ka) scoria cone of the Sacrofano caldera (Sottili *et al.* 2010), but glass geochemical datasets for these activities are not available. Thus, a precise correlation of TF-64b cannot be provided at this time.

TF-68 /-69 ($^{40}\text{Ar}/^{39}\text{Ar}$ ages 329.2 ± 3.4 ka/331.9 ± 1.0 ka). – Tephra layers TF-68/69 share a similar, phonolite-dominated composition, but can be distinguished based on lithological and geochemical differences. TF-69 shows a wider geochemical spectrum including also less evolved tephritic–phonotephritic–tephriphonolitic glass compositions and has a twofold

lithological zonation with a greyish-whitish bottom and a black top subunit (Table 1). TF-68 instead includes more evolved tephriphonolitic and trachytic components and a twofold lithological zonation (Table 1) with a fine-grained whitish bottom and coarse-grained, normal-graded greyish top unit. Within the CaO/FeO vs. Cl diagram both layers plot within the fields of the Vico volcano, the SVD and the VVD, with the majority of analyses indicating an origin from the latter (Fig. 3F). TF-68/-69 have been individually $^{40}\text{Ar}/^{39}\text{Ar}$ dated yielding weighted mean ages of 329.2 ± 3.4 and 331.9 ± 1.0 ka, respectively. The Vulsini-like geochemical fingerprint and the ages suggest a correlation with the Bolsena–Orvieto explosive cycle of the VVD (Palladino *et al.* 2014). A geochemical comparison of TF-68/-69 with the Orvieto–Bagnoregio eruption (WOB) reveals a good geochemical match of the more evolved compositions, but also demonstrates the wider compositional spectrum of TF-68/-69, including the less evolved compositions (Figs 4D–F, S1C, D). Within the TAS diagram, the WOB composition shows a narrow phono-trachytic trend (Palladino *et al.* 2014), which is wider and more evident in TF-68 than in TF-69 (Fig. 4D). However, considering all other element compositions, the geochemistry data do not allow an unambiguous preferable correlation (Figs 4D–F, S1C, D). The ages for the WOB eruption products range between 307 and 335 ka (Turbeville 1992; Nappi *et al.* 1995; Marra *et al.* 2020b), whereof Marra *et al.* (2020b) suggest an age of 335.5 ± 1.5 ka for the main eruptive event, which is close to those of TF-68/-69. The bottom units of the WOB deposits described in proximal settings consist of whitish-light grey pumice Plinian fallout and flow deposits rich in sanidines, which are overlain by a unit of moderately vesicular, dark grey–black scoria blocks very rich in leucites (Palladino *et al.* 2014). The same pattern is observed for TF-69 (bottom sanidines, top leucites, Fig. 2). Along with its slightly older age, a correlation of TF-69 with the main eruptive phase of WOB is proposed. Thus, the slightly younger layer TF-68 most likely corresponds to the subsequent WOB activity, which is also evident in the scattering ages obtained on proximal deposits (Marra *et al.* 2020b) and Fucino tephra layers TF-66/-67.

TF-71 (modelled 338.5 ± 1.7 ka). – The glass composition of tephra TF-71 is mainly phonolitic, but also encompasses some tephriphonolitic glasses with relatively high $\text{K}_2\text{O}/\text{Na}_2\text{O}$ ratios between 1.5 and 3.1 (Fig. 4E). Within the CaO/FeO vs. Cl diagram, TF-71 plots in the overlapping fields of the SVD and VVD similar to TF-68 and -69 (Figs 3F, 4D–F). No explosive volcanic activity is known from the SVD at that time, but the age of TF-71 falls between two active pulses of the VVD. TF-71 is slightly older than the oldest weighted mean ages given for the WOB activity (331–335 ka) and slightly younger than those of the Ponticello Pumices

(347–351 ka; Nappi *et al.* 1995; Marra *et al.* 2020b). Following the approach of Marra *et al.* (2020b) to identify previously undefined eruptions by assessing all single crystal ages of different proximal units within the VVD, an age cluster of 337.9 ± 1.2 ka (CB3 cluster) overlaps with the age of TF-71. Unfortunately, no geochemical data are available to verify the supposed correlation. Crystal populations of similar age were also described in different sites of the VVF, but has not been associated with a known explosive volcanic event so far (PO-C6: 338.3 ± 6.4 ka, Marra *et al.* 2021b). However, the distinctive geochemical features of VVF products rule out a possible correlation. Owing to the strong similarity of TF-71 with the slightly younger WOB equivalents (Figs 4D–F, S1C, D), a correlation with an undetermined eruption predating the WOB eruption of the VVD appears more likely.

Compositional Group 1B (CG1B). – Tephra layers TF-65, -83 and -84 belong to the compositional group CG1B, which contains poorly evolved compositions, including tephrites, shoshonites and phonotephrites, as well as SiO_2 -poor foidites (Fig. 3A, D). TF-65 is characterized by a relatively low $\text{K}_2\text{O}/\text{Na}_2\text{O}$ ratio of ~ 1.2 , whereas TF-83 and TF-84 have mean alkali ratios of 1.8 and 2.2, respectively. Owing to the low mean SiO_2 concentrations (44–51 wt%) of CG1B tephra layers, the CaO/FeO vs. Cl diagram can only be used tentatively for exploring their volcanic origin (Giaccio *et al.* 2019). TF-65, -83, and -84 have low Cl concentrations and relatively high CaO/FeO ratios, indicating a Roman Province origin plotting in similar positions of the SVD and VVD fields.

TF-65 (modelled age 320.8 ± 3.3 ka). – TF-65 has a main tephritic–foiditic composition (mean $\text{K}_2\text{O}/\text{Na}_2\text{O} = 1.15$), which is accompanied by a second minor foiditic shard (cf. Fig. 3D). The major element compositions of the second population are clearly Na-dominated ($\text{K}_2\text{O}/\text{Na}_2\text{O} = 0.7$) and have significantly higher Al_2O_3 and lower TiO_2 , MgO and CaO concentrations compared with the main population (Fig. S2). Based on the CaO/FeO vs. Cl discrimination, most shards of the main population indicate an origin from the SVD, whereas some plot in the VVD field (Figs 3G, S2). The Bracciano–Sacrofano volcanic activity of the SVD is of similar age (Sottili *et al.* 2010), but has not been geochemically investigated because of strong thermal alteration and/or zeolitization (cf. similar aged TF-64b). The main eruptive event, the Tufo di Bracciano, is described as a major caldera-forming eruption (Sottili *et al.* 2010), which suggests a more differentiated composition similar to other main SVD eruptions (Marra *et al.* 2014), such as the one of TF-65. The subsequent minor volcanic activity of the scoria cones Monte Musino and Monte Rocca Romana (319.1 ± 6.0 ka, 320.1 ± 14.0 ka, respectively; Sottili *et al.* 2010) may be a potential source for TF-65.

TF-83/84 (modelled 365.3 ± 3.0 ka; 365.5 ± 2.9 ka). – TF-83 has a homogeneous tephritic main composition and some foiditic–tephritic shards (Fig. 5A). The tephrites are characterized by higher mean concentrations in MgO (7.98 wt%), CaO (15.31 wt%) and K_2O/Na_2O ratios (1.92), whereas the foiditic–tephritic shards have mean values of 6.46 wt%, 14.32 wt% and 1.39 respectively. TF-84 has a tephritic–phonotephritic–shoshonitic composition, which is accompanied by foidite–tephrite–phonotephrites. Although both TF-84 compositional groups differ in their alkali ratio, with the latter having a mean alkali ratio of 1.48 and a major group of 2.65, the other elemental compositions with regard to their SiO_2 content lie on the same evolutionary trend and suggest a common volcanic source.

Volcanic activity with low evolved compositions and/or SiO_2 -poor is reported for the VVF, Roccamonfina

and CAVD at that time. At the VVF, the Selva Piana products are of similar age (362.4 ± 11.0 ka, Boari *et al.* 2009b), but do not show high K series compositions. The BLT stage marks the end of the HKS phase of the Roccamonfina volcano, but whole-rock compositions of similar aged lavas (RMF4, RMF3, 89X, RMF7; 369–355 ka; Rouchon *et al.* 2008) slightly differ in their geochemical compositions (more evolved HKS-type lavas, slightly younger KS-lavas, Fig. 5A–C). Minor (strombolian and hydromagmatic) activity of post-calderic centres within the CAVD marks the end of the Tuscolano–Artemisio phase with the deposition of the Madonna degli Angeli succession, whose products have been dated between 355 and 366 ka (Table 3; Karner *et al.* 2001; Marra *et al.* 2003; Gaeta *et al.* 2006; Sottili *et al.* 2009; Gaeta *et al.* 2016). However, the precise chronostratigraphy of the post-caldera activity

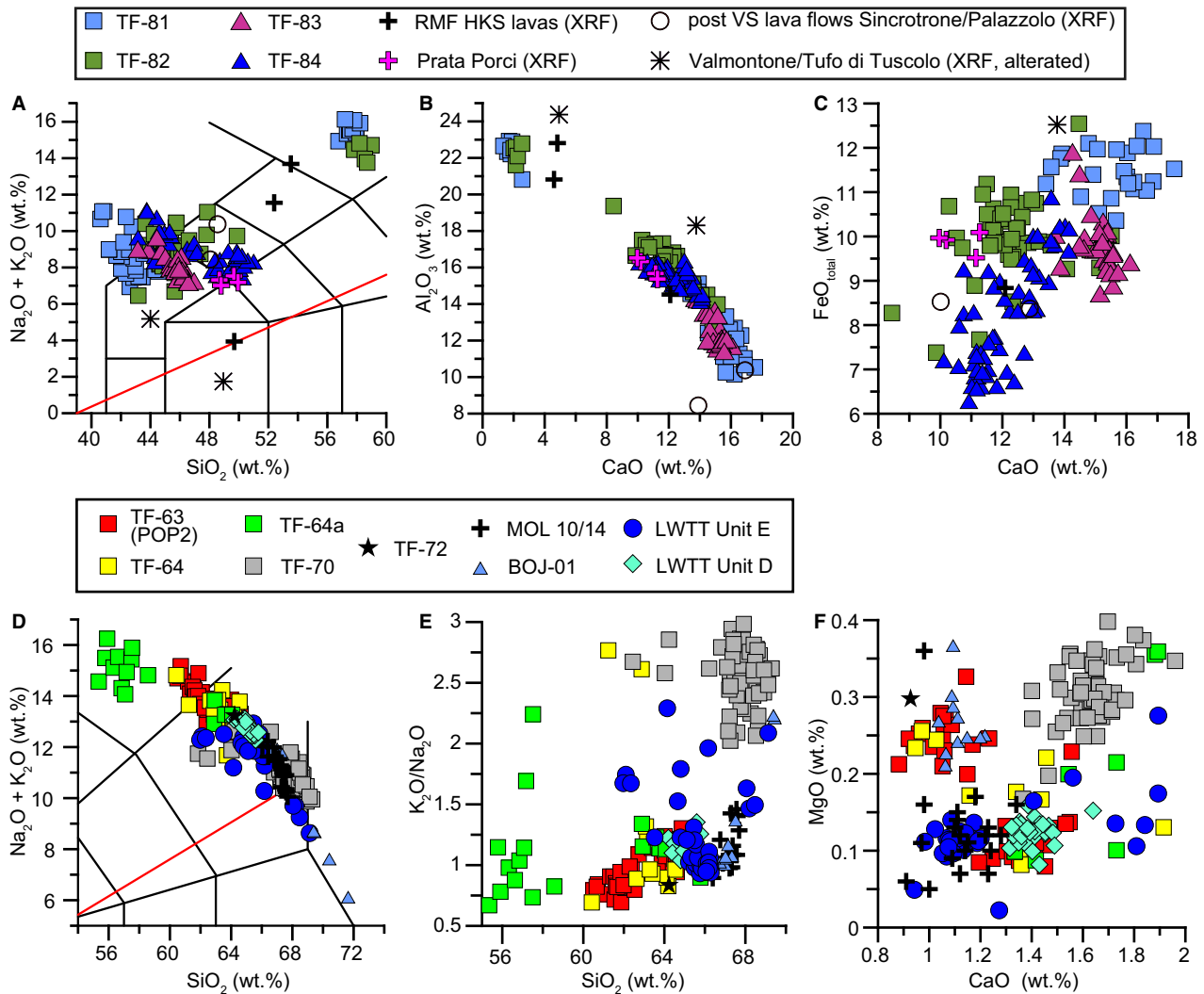


Fig. 5. TAS diagram and bi-variate plots of tephra layers associated with the CAVD and Roccamonfina volcano. A–C. Comparison of TF-81/82/83/84 with XRF data of HKS lavas from Roccamonfina (Rouchon *et al.* 2008) and with XRF compositions of the post VS caldera activity from the CAVD (Sottili *et al.* 2012; Gaeta *et al.* 2016; Marra *et al.* 2016b). D–F. Comparison of TF-63/64/64a/70/72 with new EPMA-WDS data for Units E and D of the WTT and from distal WTT equivalents (MOL 10/14, BOJ-01) found in the Bojano basin (Amato *et al.* 2014; Galli *et al.* 2017).

remains unknown, as ages are indistinguishable within uncertainties among themselves and from the age of the Villa Senni eruption (Marra *et al.* 2009). Whole rock geochemical compositions of associated lava flows (Marra *et al.* 2011; Gaeta *et al.* 2016) and from Prata Porci (Sottili *et al.* 2009) suggest a similar composition to TF-83/-84 (Fig. 5A–C). Within the uncertainties related to the comparison of whole-rock vs. glass data, the composition of TF-83/-84 is in good agreement with those of deposits of Prata Porci, which have been dated at 366.1 ± 1.2 ka (Marra *et al.* 2016b). In addition, the temporal vicinity of the Villa Senni eruption that is found just below TF-83/-84 (TF-85: 365.8 ± 1.8 ka; Giaccio *et al.* 2019; Monaco *et al.* 2021) further supports a tentative correlation.

Compositional Group 1C (CG1C). – Tephra layers TF-66/-67/-74a/-74d/-75/-77/-78/-79 form compositional group CG1C with intermediate compositions between CG1A and CG1B. These tephra layers have a dominant tephriphonolitic and/or phonotephritic composition with minor amounts of shards and show a more evolved phonolitic or less evolved tephritic composition. TF-74a/-74d/-75/-77 are mostly Na dominated with K_2O/Na_2O ratios ≤ 1 , whereas the other tephra layers have alkali ratios between 1.30 and 1.75. Within the CaO/FeO vs. Cl diagram, the tephra layers plot in the Roman Province fields with some tendency towards the Roccamonfina field (Fig. 3H).

TF-66/-67 (modelled ages $327.5 \pm 3.0/328.5 \pm 2.8$ ka). – TF-66/-67 are two distinct tephra layers with no indication of reworking of the younger TF-66. They have a similar age and occupy an almost identical position within the tephriphonolitic field of the TAS diagram, with some data scattering in the phonotephritic and shoshonitic fields (Fig. 4D–I). The similarity is also seen in the other elemental compositions and lithological characteristics (Figs 4D–F, S1C, D; Table 1). The CaO/FeO vs. Cl diagram suggests an origin from the SVD or VVD (Fig. 3H). Potential eruptions are the slightly younger Tufo di Bracciano from the SVD (cf. TF-64b/-65/-65a; 310–324 ka; Sottili *et al.* 2010; Pereira *et al.* 2017) and eruptive events associated with the post-WOB activity of the VVD (cf. TF-68/-69; Marra *et al.* 2020b) dated at 328.2 ± 3.5 (youngest population in CB2) and 329.4 ± 1.6 ka (CB-260). The better chronological match tentatively suggests a correlation of TF-66/-67 with the VVD eruptions, but this needs to be validated by geochemical data once available.

TF-74a/-74d/-75/-77 (modelled 347.4 ± 3.5 ka; 347.8 ± 3.6 ka; 351.7 ± 3.6 ka $^{40}Ar/^{39}Ar$ of TF-75 350.9 ± 3.0 ka). – TF-74a/-74d/-75/-77 form a cluster of tephra layers occurring in a narrow time interval of *c.* 3.5 ka and they share similar phonotephritic–tephriphonolitic compositions (Fig. 6A) with low alkali ratios. The entire

cluster covers a wide spectrum in the TAS diagram, with silica ranging from 45 wt% (especially TF-74a) to 55 wt% (Fig. 6A). TF-74a has a tephritic, phonotephritic-dominated composition (mean $K_2O/Na_2O = 1.0$) overlapping with that of TF-74d, for which only two phonotephritic ($K_2O/Na_2O = 0.5$) and one trachyandesitic shard ($K_2O/Na_2O = 0.9$) have been analysed. The compositions of TF-75/-77 are mainly phonotephritic–tephriphonolitic, of which the one of TF-75 also reaches the tephritic field, with both layers having a mean K_2O/Na_2O ratio of 0.9. TF-74a/-75/-77 plot in a similar overlapping position between the SVD and Roccamonfina fields within the CaO/FeO vs. Cl diagram, whereas TF-74d plots in both the Vico and Roccamonfina fields (Fig. 3H). Owing to the volcanic inactivity of the SVD and the Vico volcano between 330 and 440 ka (Marra *et al.* 2020a) and between 305 and 390 ka (Perini *et al.* 2004; Monaco *et al.* 2021), respectively, a Roman source appears unlikely. From the Volsci Volcanic Field, eruptions with ages of 347.2 ± 4.3 ka (CA-C1, Marra *et al.* 2021a) and 351.8 ± 4.0 ka (K-layer, Nomade *et al.* 2011) are described, but the limited geochemical characterizations of Volsci compositions differ (Boari *et al.* 2009b). From the Roccamonfina volcano, the BLT sequence is imprecisely framed between 344 and 353 ka (Rouchon *et al.* 2008; Scaillet *et al.* 2008; Santello 2010). Luhr & Giannetti (1987) and Santello (2010) described these deposits ranging from tephritic to phonolitic in composition, similar to those observed for TF-74a/-74d/-75/-77 (Fig. 6A–E). Their low alkali ratios, and especially those of TF-74d, match those observed for the BLT pumices with CaO > 5.6 wt%. The BLT pumices show increased Na/K ratios owing to the analcimization of leucite (Luhr & Giannetti 1987). However, the analcimization of proximal deposits and weathering, as expressed by high loss on ignition values (7–10%), limit any tentative geochemical correlation between the whole-rock XRF data and the single-grain EPMA-WDS data. Nevertheless, these data demonstrate that also less evolved composition could be associated with the BLT. Based on the chronological and general geochemical similarities with the eruptions associated with the BLT sequence, the origin of TF-74a/-74d/-75/-77 is presumably the Roccamonfina volcano. The $^{40}Ar/^{39}Ar$ age of 350.9 ± 3.0 ka obtained for tephra layer TF-75 matches those obtained for proximal BLT deposits (352.0 ± 5.0 ka, Rouchon *et al.* 2008; 347.7 ± 11.2 ka, Scaillet *et al.* 2008; 352.3 ± 3.0 and 352.4 ± 3.0 ka, Santello 2010) and those of a tephra layer in the archaeological site of Guado San Nicola that was tentatively attributed to the BLT phase (S.U. Tufi: 343.9 ± 5.2 , Pereira *et al.* 2016).

In distal settings, a similar wide compositional tephrite to evolved tephri-phonolite spectrum is observed for the BAG tephra (Fig. 6A). This tephra is a widespread marker horizon found in several Loess Palaeosol sequences of the Danube basin in eastern Europe

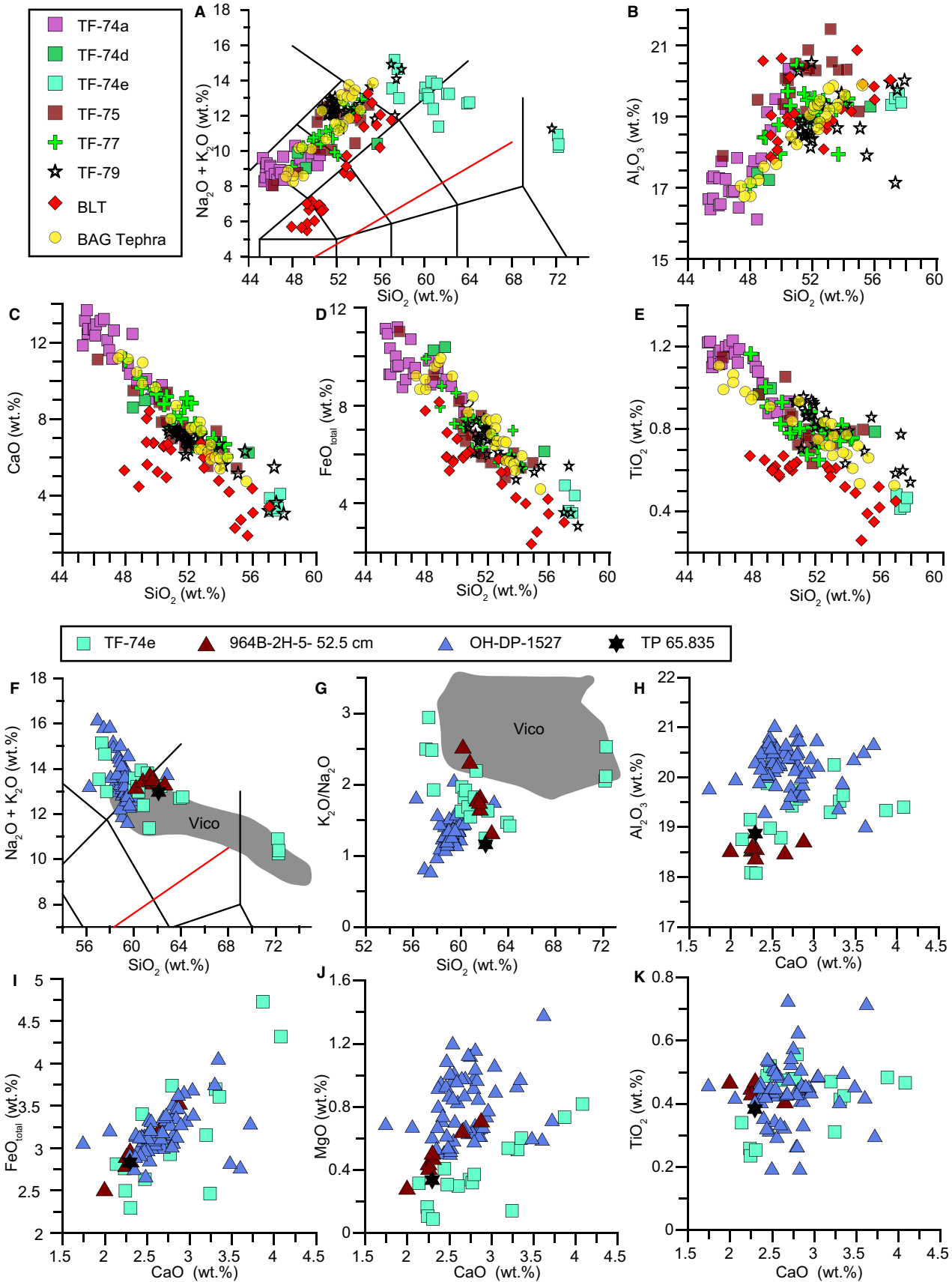


Fig. 6. TAS diagram and bi-variate plots of tephra layers associated with the BLT of the Roccamonfina volcano and distal equivalents. A–E. Comparison of TF-74a/-74d/-74e/-75/-77/-79, the XRF based composition of the BLT (Luhr & Giannetti 1987; Santello 2010) and the EPMA-WDS data of the BAG tephra (Poulet et al. 1999). F–K. Comparison of TF-74e and discussed potential equivalents found in the marine site ODP964B (Vakhrameeva et al. 2021), the Lake Ohrid succession (Leicher et al. 2021) and the Tenaghi Philippon record (Vakhrameeva et al. 2018).

(Fig. 1, Poulet et al. 1999; Laag et al. 2021; Jordanova et al. 2022). Previous correlations of the BAG tephra with the Villa Senni eruption have been disproven by Monaco et al. (2021), who proposed an alternative correlation with the older F4–F5 tephra cluster TF-102/106 (397–399 ka). However, new chronostratigraphical information of the BAG tephra in both the Zenum and Suhia Kladenetz sequences (Laag et al. 2021; Jordanova et al. 2022) suggests a deposition in MIS 10 glacial deposits, which is in conflict with the position of the TF-102/106 tephra during MIS 11. Based on the glass geochemistry obtained at the Pásztó site (Poulet et al. 1999), TF-75/-77/-79 show strong geochemical similarities with the BAG tephra (Fig. 6A–E), of which the best match is given by TF-77. Tephra T32 from the Piànico–Sèllere palaeolake sequence in northern Italy was suggested to correlate also with the BAG tephra and to be an equivalent of the BLT eruptive series (Brauer et al. 2007b). However, the age of the sequence and the supposed tephra correlation are controversially discussed (Pinti et al. 2007; Brauer et al. 2007a), as palaeomagnetic information (Scardia & Muttoni 2009) and a K–Ar age of an underlying tephra (779 ± 13 ka, Pinti et al. 2001) suggest deposition of the sequence within MIS 19. Further, isotopic analyses of T32 rather suggest the palaeo-SVD as the volcanic source (Rouilleau et al. 2009; Sottili et al. 2019). This is further corroborated by a proposed correlation with tephra SUL2-11 from the Sulmona MIS 19 deposits (Giaccio et al. 2015a), which was also assigned to the palaeo-SVD activity (Sottili et al. 2019).

TF-78 (modelled age 353.2 ± 3.6 ka). – Tephra layer TF-78 has a mainly phonotephritic–tephriphonolitic composition with some basaltic–trachyandesitic and andesitic components (Fig. 4G). The alkali ratio increases from 0.8 to 3.1 with increasing SiO₂ content, and MgO concentrations are higher and Al₂O₃ lower compared with the generally similar TF-74a/-75/-77 tephra layers. Therefore, a correlation with the BAG tephra found in Hungarian loess deposits appears unlikely (cf. TF-75/-77/-79; Fig. S3). Based on the CaO/FeO vs. Cl diagram an origin from the Roman Province is likely, with most data plotting within the field of the VVD (Fig. 3H). The Ponticello Pumices is a major Plinian fall eruption from the Bolsena area of the VVD and dated at 350.9 ± 4.0 ka (Nappi et al. 1995), whereas a more recent dating is showing a significantly younger age (346.6 ± 1.4 ka, Marra et al. 2020b). Although white pumice lapilli are described as trachytes (Nappi et al. 1994), these deposits also contain a mafic component that could match the less evolved composition of TF-78. However, with respect to

the age discrepancy, TF-78 is classified as an undefined eruption associated with the VVD, which is also possibly represented by ⁴⁰Ar/³⁹Ar dated volcanoclastic deposits found in archaeological and Tiber valley sections south of the Roman volcanoes (TOR1 + POL12-02, 353.5 ± 4.0 ka; CH-AF, 350.8 ± 1.7 ka, Marra et al. 2016a).

TF-79 (modelled age 355.1 ± 3.6 ka). – Tephra layer TF-79 is composed of tephriphonolites and phonolites with mean alkali ratios of 1.3 and 1.5, respectively. A single high K-rhyolitic shard with a high alkali ratio of 3.8 and distinct different geochemistry suggests a second volcanic source (cf. Single shard compositions of tephra layers TF-65/-72/-79). The main population of TF-79 plots within the Roccamonfina field of the CaO/FeO vs. Cl diagram, but some data scatter in the Roman fields (Fig. 3H). The age of TF-79 matches the BLT activity (348–355 ka; Rouchon et al. 2008; Scaillet et al. 2008; Santello 2010) from the Roccamonfina volcano. Considering for a general comparison the limited whole rock and matrix XRF data available for the BLT (Luhr & Giannetti 1987), the phonolitic part of TF-79 overlaps with the evolved composition described for the BLT (Fig. 6A–E). Moreover, the similarity to TF-74a/-75/-77 and their common position within the CaO/FeO vs. Cl diagram (Fig. 3H) strengthen the tentative correlation of TF-79 with an early BLT phase of the Roccamonfina volcano. Luhr & Giannetti (1987) described deposits from a Plinian eruption, directly underlying those of the BLT eruption, which may represent a potential counterpart for TF-79. As discussed for TF-75/-77, TF-79 is another potential equivalent of the BAG tephra, although its compositional spectrum is shifted towards more evolved compositions (SiO₂ 50–58 wt%), compared with the less evolved BAG composition (SiO₂ mainly 48–54 wt%) (Fig. 6A–E).

Compositional group 2 (CG2)

Tephra layers TF-64/-64a/-70/-72/-74e form compositional group CG2 and plot along a phonolitic–trachytic–rhyolitic trend, discriminating them from CG1 tephra layers. CG2 tephra layers comprise both low and high alkali ratio (LAR < 1.5 > HAR) trachytes and show within the CaO/FeO vs. Cl diagram similarity to the Campanian and Roccamonfina compositions, except some data with low CaO/FeO ratios plotting in the Roman Province fields (Fig. 3J). The origin of TF-72 is discussed in the chapter ‘Single shard compositions of tephra layers TF-65/-72/-79’, as only one shard could be analysed. The volcanic activity of the Campanian

Province preceding the Campanian Ignimbrite eruption (>40 ka; Giaccio *et al.* 2017b) is only fragmentarily documented and the precise volcanic origin of older products within the Campanian Province remains unclear at present (Rolandi *et al.* 2003; Wulf *et al.* 2004; Munno & Petrosino 2007; Paterne *et al.* 2008; Wulf *et al.* 2012; Petrosino *et al.* 2014; Leicher *et al.* 2019, 2021; Vakhrameeva *et al.* 2021; Monaco *et al.* 2022a). However, some widespread Mediterranean tephra were recently correlated with Plinian deposits found in the Campanian Plain and attributed to a Campi Flegrei activity of 92–109 ka (Monaco *et al.* 2022a), suggesting that the Campi Flegrei was probably the source of the Campanian Province-like tephra of the Middle Pleistocene. Known volcanic activity in the age range of CG2 tephra layers (316–348 ka) is also reported for the Roccamonfina volcano with the emplacement of two main eruptive sequences of the BLT and WTT (Giannetti & De Casa 2000; Rouchon *et al.* 2008).

TF-64/-64a (modelled ages 316.0±2.9 ka / 316.2±2.9 ka). – TF-64 has a mainly LAR-type trachytic composition (mean $K_2O/Na_2O = 0.98$) with a minor phonolitic component and is further characterized by low CaO concentrations (mean = 1.3 wt%). TF-64 plots within the CaO/FeO vs. Cl diagram in the compositional fields of Ischia and Campi Flegrei (Campanian Province), with some data scattering also in the Roccamonfina field (Fig. 3J). TF-64a has a phonolite-dominated composition with only few shards classified as trachytes and a mean alkali ratio of 0.9. Trachytic shards plot within the CaO/FeO vs. Cl diagram in the field of the Campanian Province, whereas phonolites both plot in Roccamonfina and Vico fields (Fig. 5D–F). The trachytic geochemical composition is very similar to the composition of the closely overlying (<3 cm distance) TF-64, which may suggest a dislocation of some shards either by bioturbation or by drilling disturbances. Volcanic activity with the age of TF-64/-64a from the aforementioned sources is only known from the Lower WTT eruptive series of the Roccamonfina volcano, from which units A–D (313–331 ka; Quidelleur *et al.* 1997; Giannetti & De Casa 2000) match from a chronological perspective. Glass geochemical compositions of proximal deposits are only available for the here investigated WTT Units E and D (306.7±5.0–312.9±4.0 ka, Giannetti & De Casa 2000). Additional glass geochemical data are given by distal equivalents of the WTT (312.1±5.0 ka, MOL12/13, BOJ-01) identified in the Bojano basin (Amato *et al.* 2014; Galli *et al.* 2017), but they have not been assigned to a specific WTT unit yet. The geochemical composition of the WTT products is similar those of TF-64/-64a (Figs 5, S4D–F), which supports their general assignment with the eruptive sequence of the Lower WTT, including Units A, B, C and D (Giannetti & De Casa 2000). Specifically, the composition of TF-64/-64a suggests a tentative correla-

tion with Unit D, despite some differences in geochemistry (e.g. wider compositional spectrum of TF-64/-64a, Fig. 5D–F). On the other hand, the Bojano WTT equivalents (MOL12/13, BOJ-01; Amato *et al.* 2014; Galli *et al.* 2017) have a more evolved composition, similar to that of the WTT Unit E (Fig. 5D–F). A correlation of MOL12/13, BOJ-01 with Unit E is further supported by their younger ages of 312.1±5.0 ka (Amato *et al.* 2014) and 307–310 ka (Giannetti & De Casa 2000), respectively.

TF-70 (modelled age 335.7±3.0 ka). – TF-70 has a mainly high-silica trachytic composition (mean $SiO_2 = 67.8$ wt%, $CaO = 1.6$ wt%) but includes also few less evolved trachytes (mean $SiO_2 = 62.8$ wt%, $CaO = 2.7$ wt%). TF-70 has the highest alkali ratios among CG2, being HAR-type trachytes with means of 2.5 and 2.9, respectively. The CaO/FeO ratios 0.4–0.7 are in then range of known Campanian Province and Roccamonfina products (Fig. 3J). However, TF-70 has Cl concentrations between 0.02 and 0.07 wt% which are untypically low for these volcanic sources and are rather known for Roman products. Among the Roman volcanic sources, the Vico volcano is the only known source for highly evolved trachytic–rhyolitic compositions (Perini *et al.* 2004; Pereira *et al.* 2020; Monaco *et al.* 2021), but the other elemental compositions are different. Moreover, no eruptive events are known for the Vico volcano in the time period of interest (Perini *et al.* 2004), which questions this volcano as the potential source. Considering the activity of the Roccamonfina volcano, the age of the oldest deposits of the WTT is discussed as being between 322.0±4.0 ka for Unit A (Giannetti & De Casa 2000) and 331.5±2.0 ka for an undefined unit (Quidelleur *et al.* 1997; Rouchon *et al.* 2008). For those deposits no glass compositions are available, but some high-silica trachytes have been associated with the younger Unit E of the WTT (this study and Amato *et al.* 2014; Galli *et al.* 2017). If those are compared with TF-70, the latter shows different compositional trends with lower Al_2O_3 and higher CaO, FeO, MgO and K_2O/Na_2O values at a given SiO_2 concentration (Figs 5D–F, S4D–F). Therefore, only a tentative correlation of TF-70 with the undefined above-mentioned WTT unit is proposed based on general WTT geochemical similarities and chronological constraints.

TF-74e (modelled age 348.3±3.6 ka). – Tephra TF-74e has a mainly phonolitic–trachytic composition, but also includes three rhyolitic shards (Fig. 3I). Phonolites and trachytes have relatively high alkali ratios of between 1.2 and 2.9, together with high CaO concentrations (2.1–4.1 wt%). Rhyolites are also characterized by high K_2O/Na_2O ratios (mean = 2.2) and a mean CaO concentration of 1.6 wt%. Bivariate element plots suggest that both groups form a compositional trend and thus belong to the same volcanic source, even if the

low number of rhyolitic shards and missing intermediate compositions hamper an unambiguous correlation. Within the CaO/FeO vs. Cl diagram, TF-74e plots both in the Vico and Roccamonfina fields (Fig. 3J). The ultrapotassic character with a rhyolitic endmember of TF-74e resembles that of older Vico products (Monaco *et al.* 2021), but an origin from the Vico volcano appears unlikely, as there is no evidence for activity in proximal and distal archives between 305 and *c.* 400 ka (Perini *et al.* 2004; Monaco *et al.* 2021). Further, Na₂O and K₂O concentrations of Vico Period I products are respectively lower and higher compared with TF-74e (Fig. 6G). The age of TF-74e matches that of the BLT eruption from the Roccamonfina volcano, and together with their general compositional similarity (Luhr & Giannetti 1987), a correlation with this eruption is tentatively proposed, as discussed for adjacent tephra layers TF-74a/-74d/-75/-77.

Within the Mediterranean tephrostratigraphical framework tephra layers ODP964B 2H-5-52.5 from the Ionian Sea (340 ka, Vakhrameeva *et al.* 2021), TP09-65.835a from Tenaghi Philippon (358 ka, Vakhrameeva *et al.* 2018) and OH-DP-1527 from Lake Ohrid (358 ka, Leicher *et al.* 2019) have similar geochemical characteristics to TF-74e (Fig. 6F–K). However, a correlation of TF-74e with OH-DP-1527 and TP09-65.835a is in conflict with the supposed 10 ka older ages and compositional variations of OH-DP-1527 (e.g. >Al₂O₃, MgO, Cl) and TP09-65.835a (>MnO, Cl). Although ODP964B 2H-5-52.5 also has higher MgO and Cl values and is slightly younger compared with TF-74e (Fig. 6F), their overall similarities suggest a tentative correlation.

Compositional group 3 (CG3)

Compositional group 3 comprises tephra layers with bimodal compositions, whose individual geochemical populations share features of different compositional groups described before. Tephra TF-63 has two populations that have CG1B and CG2 characteristics, whereas populations of tephra layers TF-65a/-76/-81/-82 show a mix of CG1A-C characteristics.

TF-63 (modelled age 315.3 ± 2.8 ka). – Tephra layer TF-63 has a twofold composition (Fig. 3K) with a CG1B-type and a CG2-type geochemical population (Figs 5, 6). The CG1B-type population (POP1) follows a tephritic–phonolitic trend dominated by phonotephritic shards, has K₂O/Na₂O ratios between 0.8 and 1.4 and plots within the Roman Province field (SVD, VVD) of the CaO/FeO vs. Cl diagram (Fig. 3L). The second population (POP2) is made up of phonolitic–trachytic shards (CG2-type) with K₂O/Na₂O ratios between 0.7 and 1.14, which indicate an origin from the Campanian or Roccamonfina volcanoes within the CaO/FeO vs. Cl diagram (Fig. 3L). Based on the different compositional trends of CG1B and CG2 type populations and thus their

supposed different volcanic origins, TF-63 most likely represents two volcanic events of similar age that were mixed. The CG1B-type tephra is compatible with the low-evolved compositions of the overlying TF-62, which is correlated with the MRPF eruption of the SVD (Figs 4A–C, S1A, B). Owing to the geochemical and chronological similarity, population 1 of TF-63 may represent a pre-eruption phase of the main MRPF eruption. Population 2 of TF-63 is similar to the compositions of underlying TF-64/-64a (Figs 5D–F, S4D–F), which have both been associated with Unit D of the WTT eruption from Roccamonfina (Giannetti & De Casa 2000). As TF-63 is stratigraphically well separated from TF-64/-64a, this may indicate that the WTT Unit D could include at least two eruptive phases, which were separated by a short time span of less than one millennium.

TF-65a (modelled age 325.3 ± 3.1 ka). – Tephra layer TF-65a has a trachytic–phonolitic, CG1A-type main population (mean alkali ratio = 1.5) and a second minor population of foidites and phonotephrites similar to those of CG1B/C (mean alkali ratio = 0.9). The structure of the tephra layer is affected by drilling disturbances, which do not allow assessment of whether the different populations may refer to individual layers or may represent a zonation of a single layer. However, bivariate element plots suggest an evolutionary trend between both populations, indicating a common volcanic source (Fig. S2). Based on their CaO/FeO ratios and Cl concentrations, a common origin from the SVD is most likely (Fig. S2). The age of TF-65a (325 ka) is within the uncertainties of the oldest age obtained for the Tufo di Bracciano eruption (cf. TF-64b; 323.9 ± 2.0 ka; Pereira *et al.* 2017). However, the scarcity of glass geochemical data from proximal SVD equivalents hampers a more reliable correlation.

TF-76 (modelled age 350.9 ± 3.6 ka). – Tephra layer TF-76 has a twofold composition (Figs 3K, 4G–I) comprising one tephritic–phonotephritic population (CG1B-type, mean K₂O/Na₂O = 1.2) and a second phonolitic–trachytic one (CG1A-type, mean K₂O/Na₂O = 2.3, CaO = 2.39 wt%). Both populations plot within the Vico and VVD fields of the CaO/FeO vs. Cl diagram, similar to the slightly older TF-78 suggesting a common volcanic source (Fig. 3L). Further, both tephra layers fall in the same compositional trend, which differs from the one of the similar aged tephra group associated with the Roccamonfina volcano (TF-74a/-74d/-75/-77: <MgO, FeO; >Na₂O, Cl). The Ponticello Pumices are the only described eruption in proximal settings of the VVD with a similar age to TF-76, being K/Ar dated at 350.9 ± 4.0 ka (Nappi *et al.* 1995), whereas ⁴⁰Ar/³⁹Ar methods suggest a more precise age of 346.6 ± 1.4 ka (Marra *et al.* 2020b). Nappi *et al.* (1994) presented geochemical data (whole-rock XRF) of white pumices of the Ponticello Pumices

eruption, which match the trachytic glass composition of TF-76 (Figs 4G–I, S3). However, a comparison of whole-rock XRF data with single-grain EPMA-WDS data may be biased by the influence of phenocrysts (Tomlinson *et al.* 2012) and the ages only partly overlap. A precise correlation of TF-76 therefore remains to be clarified.

TF-81/82 ($^{40}\text{Ar}/^{39}\text{Ar}$ ages 362.7±5.0 and 362.8±3.2 ka). – Tephra layers TF-81 and TF-82 both have a similar geochemical pattern comprising a less evolved CG1B-type population and a more evolved CG1A-type one (Figs 3K, 5A). The CG1B type population of TF-81 is foiditic–tephritic in composition, whereas that of TF-82 has a slightly more evolved foiditic–tephritic–phonotephritic composition. TF-82 has higher Al_2O_3 and lower FeO, CaO, MgO concentrations (Figs 5A–C, S4A–C), whereas alkali ratios of 1.3 and 1.5, respectively, are similar. The CG1A-type phonolitic compositions of TF-81/82 are similar, being characterized by high Al_2O_3 (22.5/22.3 wt%) and distinctive low MgO (0.09/0.11 wt%) mean concentrations and mean alkali ratios of 0.9 and 0.7, respectively. The $^{40}\text{Ar}/^{39}\text{Ar}$ ages obtained for TF-81/82 (362.7±5.0 ka, 362.8±3.2 ka) match those of volcanic products dated in the VVF (CA-CGT, 360.8±6.5 ka; Isoletta 3, 363.2±3.8 ka; ERN91, 362.4±11.0 ka; Boari *et al.* 2009b; Marra *et al.* 2021a). However, VVF deposits typically lack more evolved phonolitic compositions (Boari *et al.* 2009b). The geochemical similarity of TF-81/82 CG1B-type components with TF-83/84 and the narrow chronological cluster they form with TF-85 (Villa Senni eruption, Giaccio *et al.* 2019) suggest an origin from the post-caldera Villa Senni activity of the CAVD (Marra *et al.* 2003; Gaeta *et al.* 2016). However, the phonolitic CG1A-type composition of TF-81/82 is not common for CAVD products (Marra *et al.* 2003, 2009, 2011; Freda *et al.* 2006; Giaccio *et al.* 2013b), except for the late activity of the Albano Maar Unit 4 (*c.* 41 ka; Gaeta *et al.* 2011; Cross *et al.* 2014). An alternative origin from the Roccamonfina volcano is suggested by the position of TF-81/82 CG1A-type shards within CaO/FeO vs. Cl diagram (Fig. 3L). The BLT phase of the Roccamonfina volcano includes multiple eruptive events, which started at *c.* 440 ka and climaxed with the BLT eruptive series at *c.* 350 ka (Rouchon *et al.* 2008). Geochemical data of similar aged pre-BLT eruptive events are restricted to whole-rock data of lava flows, which generally match the primitive compositions of CG1B type TF-81/82, but also include more evolved compositions reaching the phonolitic field (undifferentiated samples in Luhr & Giannetti 1987; RMF4, RMF3, 89X; Rouchon *et al.* 2008). Differences in the geochemical composition (more evolved HKS-type lavas, slightly younger KS-lavas, Fig. 5A–C) do also not allow a robust correlation with TF-83/84. Thus, the origin of TF-83/84 cannot clearly be identified.

Single-shard compositions of tephra layers TF-65/72/79

TF-65 (modelled age 320.8±3.3 ka). – Owing to the distinctive different geochemical composition and the single-shard character, the foiditic component of the predominantly tephritic TF-65 most likely represents displaced material of a second eruption. The composition is not similar to other adjacent tephra layers of the sequence, which excludes reworking of one of these layers and rather suggests an origin from an undetected cryptotephra horizon. The Na-dominated foiditic composition is unique, but also precludes a correlation with known foiditic volcanic sources, such as the Colli Albani district or the Volsci Volcanic Range. Both source areas are characterized by high K-rocks (Boari *et al.* 2009a; Giaccio *et al.* 2013b) and were dormant at that time (Giaccio *et al.* 2013b; Marra *et al.* 2021a). Therefore, the precise chronostratigraphic position and origin of the second population remain unclear at present.

TF-72 (modelled age 340.8±3.6 ka). – For tephra TF-72 only a single shard could be analysed, being an LAR-type trachyte ($\text{K}_2\text{O}/\text{Na}_2\text{O} = 0.8$), with low CaO concentration (0.9 wt%) plotting in the compositional field of Ischia (Fig. 3J). Evidence for Middle Pleistocene volcanic activity within the Campanian Province is only provided from distal tephra layers, some of which are characterized by low-CaO, LAR trachytes. Among these LAR-type trachytes, a marine cryptotephra layer ODP964B 2H-5-67.5 from the Ionian Sea is of similar age (345 ka, Vakhrameeva *et al.* 2021), but differs in its total elemental composition from TF-72. The Roccamonfina volcano could be another potential volcanic source, since the limited available geochemical data for the slightly younger WTT deposits (307–332 ka; Quidelleur *et al.* 1997; Giannetti & De Casa 2000) are also characterized by low-CaO, LAR-type trachytes (Fig. S4D–F). Therefore, the origin of TF-72 remains unknown at present, but probably lies within the Campanian Province or the Roccamonfina volcano, predating the oldest known WTT deposits.

TF-79 (modelled age 355.1±3.6 ka). – The peculiar composition of the single rhyolitic shard from this predominantly tephriphonolitic–phonolitic tephra does not match those of similarly aged Aeolian Arc rhyolitic eruptions identified in Lake Ohrid (OH-DP-1530/1520; Leicher *et al.* 2019), as its high K-content rather suggests an origin from the Vico volcano (Perini & Conticelli 2002; Perini *et al.* 2004; Pereira *et al.* 2020). TF-79 overlaps with the compositions of older rhyolitic Vico eruptions found in the sequence (Pereira *et al.* 2020; Monaco *et al.* 2021), but also those identified in the younger TF-74e. As only a single shard was found and no volcanic activity from the Vico volcano is known from proximal and distal archives (Perini *et al.* 2004) for the time of deposition of TF-79, it

most likely represents displaced material from an unknown source.

Insights into the peri-Tyrrhenian explosive history during the 313–366 ka interval

The eruptive order of tephra layers identified in the F4–F5 site confirms the general pattern of volcanic activity observed in proximal settings (Fig. 7). The high number of identified tephra layers provides more details on the

individual eruptive sequences (Fig. 8), with two main eruptive series from the Roccamonfina volcano (*c.* 355–366 ka, 315–330 ka) and intercalated tephra layers associated with the main eruptive pulses of the Colli Albani (*c.* 365 ka), Vulsini (*c.* 330 ka and 350 ka) and Sabatini (*c.* 315–325 ka).

Based on chronological constraints and a general SVD-like geochemical character, tephra layers TF-64b, TF-65 and TF-65a were associated with the volcanic activity of the Bracciano and Sacrofano calderas of the

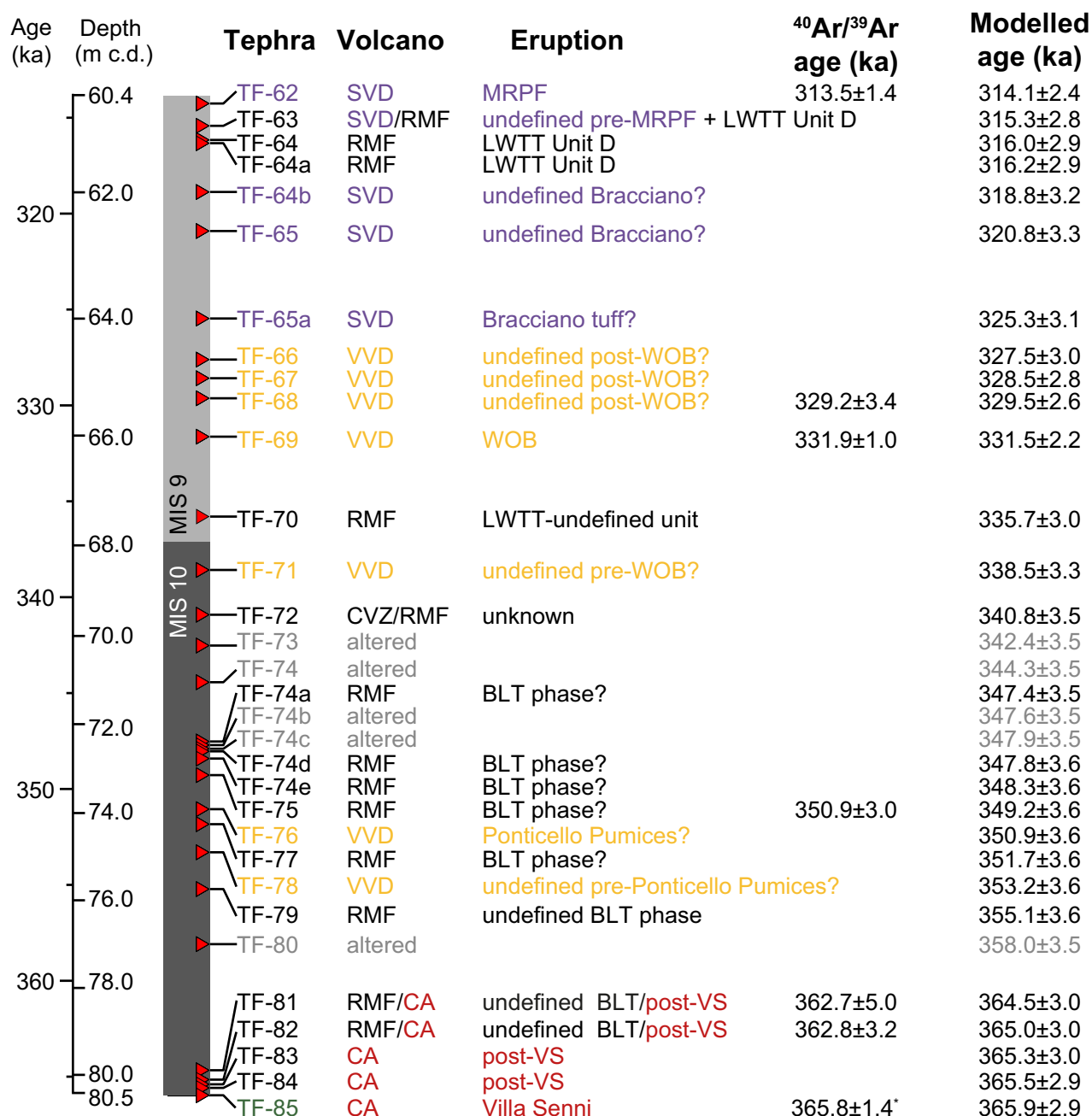


Fig. 7. Overview of the volcanic sources and chronology ($^{40}\text{Ar}/^{39}\text{Ar}$ and modelled ages) of the investigated tephra layers within the Fucino F4–F5 record. The climatostratigraphical position of tephra layers is indicated by the MIS boundaries based on Lisiecki & Raymo (2005). * Age from Monaco *et al.* (2021).

SVD between 319 and 323 ka. The Tufo di Bracciano, which is the main SVD eruptive event of this period, is chronologically scattered in proximal settings (310–324 ka; Sottili *et al.* 2010; Pereira *et al.* 2017). The oldest age matches that of TF-65a (i.e. 325.2 ± 3.1 ka), while the slightly younger deposits TF-64b/-65 (318.8 ± 2.9 ka, 320.8 ± 2.9 ka) may represent subsequent smaller events of post-caldera eruptive centres located within the Bracciano and Sacrofano area (Sottili *et al.* 2010).

The correlation of the Magliano Romano Plinian Fall with TF-62 represents the first recognition of this event in a distal archive. TF-62 provides a $^{40}\text{Ar}/^{39}\text{Ar}$ age of 313.5 ± 1.4 ka that is in agreement with the age of 312.8 ± 2.0 ka obtained on proximal deposits (Sottili *et al.* 2010). Tephra TF-63 (modelled age 315.3 ± 2.8 ka) may represent an unknown pre-MPRF event from the SVD, yet to be recognized in proximal settings.

Tephra layer TF-76 was tentatively associated with the Ponticello Pumices eruption of the Vulsini volcanic district (347–351 ka; Nappi *et al.* 1995; Marra *et al.* 2020b), but the correlation needs to be validated by a comparison with proximal geochemical data, which are currently lacking. TF-78 is a less evolved and slightly older eruption (353.2 ± 3.6 ka), potentially correlated to VVD predating the Ponticello Pumices. Furthermore, TF-69 represents the first distal equivalent recognized of the prominent WOB eruption of the VVD, which caused a caldera collapse in the sector of the Bolsena caldera (Palladino *et al.* 2014). The recognition of several similar tephra layers post- (TF-66/-67/-68) and pre-dating (TF-71) the actual WOB eruption supports the findings of Marra *et al.* (2020b), who identified several previously undefined eruptions by assessing clusters of single-crystal $^{40}\text{Ar}/^{39}\text{Ar}$ ages of pyroclastic deposits of the VVD. This supports the idea of a complex eruptive history and helps to define the age of the main WOB eruption. Marra *et al.* (2020b) identified in different deposits two clusters at 330.8 ± 1.0 ka (cluster CB-2-3-4-260) and 337.9 ± 1.2 ka (cluster CB-3), resulting in a combined age of 335.5 ± 1.5 ka (CB-3 combined) for the WOB eruption. The new findings of the Fucino sediment succession allow a better discrimination of individual eruptions. TF-69 (331.5 ± 2.2 ka) and TF-71 (338.5 ± 3.3 ka) match the two clusters identified by Marra *et al.* (2020b). TF-68 with a $^{40}\text{Ar}/^{39}\text{Ar}$ age of 329.2 ± 3.4 ka and TF-66/-67 with modelled ages of 327.5 ± 3.3 and 328.5 ± 2.8 ka postdate the WOB eruption, as also indicated by a much younger age cluster of 322.3 ± 0.9 ka (cluster CB-4-5, Marra *et al.* 2020b).

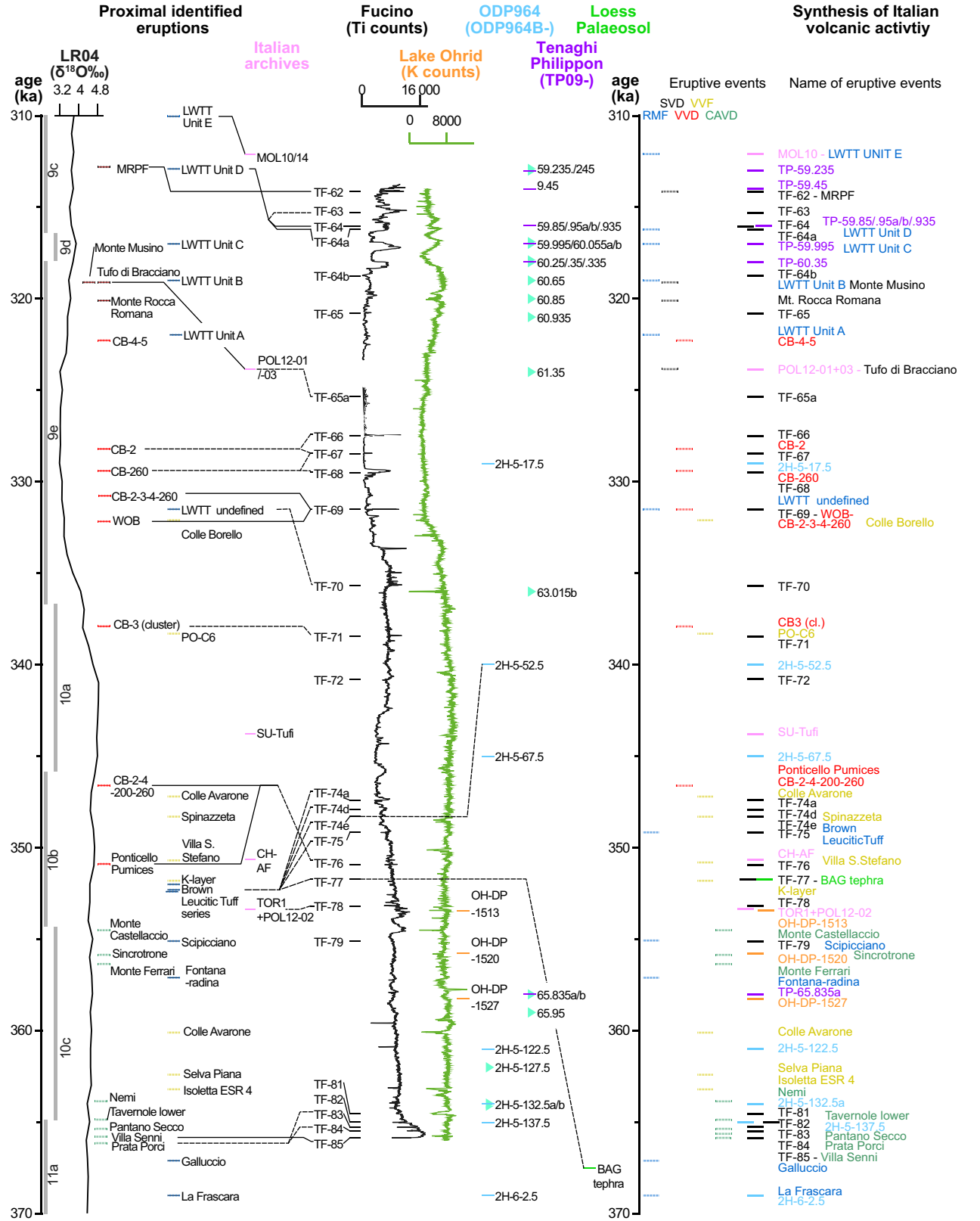
Based on the results of the Fucino sediment succession, TF-69 best represents the main WOB eruption and provides an age of 331.5 ± 2.2 ka, which is the most accurate age for WOB at present.

Tephra layers TF-83/-84 have been associated with the waning, post-caldera activity of the Tuscolano–Artemisio/Vulcano Laziale phase of the Colli Albani volcanic district (Marra *et al.* 2009, 2016b; Giordano *et al.* 2010; Gaeta *et al.* 2016). The chronology of this activity in the proximal setting was previously imprecisely constrained as the reported ages were supposedly affected by the presence of xenocrysts from the underlying Villa Senni caldera-forming eruption products, and were within uncertainties chronologically indistinguishable (Gaeta *et al.* 2016; Marra *et al.* 2016b). The finding of potential equivalents within the sedimentary succession of the F4–F5 record as distinct tephra layers, supports their proposed slightly younger age of the Villa Senni eruption, but also allows the timing to be constrained to within one millennium (Figs 7, 8).

Two tephra clusters of the F4–F5 record were associated with one of the main eruptive cycles of the Roccamonfina volcano, i.e. the BLT and the WTT stages, which have been dated in proximal settings at *c.* 355–440 ka and 307–332 ka, respectively (Giannetti & De Casa 2000; Rouchon *et al.* 2008). TF-70 from between these two main clusters was also tentatively ascribed to the WTT stage (Fig. 7). The BLT and the WTT stages document a general transitional phase of the magmatic system of the Roccamonfina volcano, which was studied intensively by whole rock data (Luhr & Giannetti 1987; Rouchon *et al.* 2008). However, glass data availability, especially for pyroclastic deposits of the BLT phase, is scarce and thus limits robust correlations at present.

The youngest cluster of tephra layers (TF-63/-64/-64a) was associated with Unit D of the WTT stage of the Roccamonfina volcano, which provides a more precise chronological constraint of the eruption between 315.3 ± 2.8 and 316.2 ± 2.9 ka for this WTT unit. However, it also shows that re-examination of the respective units is needed, as several layers related to one main eruptive unit rather indicate multiple eruptions closely spaced in time (Fig. 7). Based on the new data acquired for proximal deposits of WTT Unit E, the origin of distal tephra layers found in the Bojano basin (BOJ-01, MOL10/14) can now be clarified. This distal layer associated with the WTT Unit E has been dated at 312.1 ± 5.0 ka (Amato *et al.* 2014) and thus provides important information for reassessing the chronology of

Fig. 8. Synthesis of proximal and distal information of the volcanic history of the Italian volcanoes and the resulting tephrostratigraphical framework of the Central Mediterranean region. All $^{40}\text{Ar}/^{39}\text{Ar}$ ages from literature were recalculated according to ACs at 1.1891 Ma (Niespolo *et al.* 2017) and the total K decay constant of Renne *et al.* (2011). See also Table 3 for references and ages. The ages of tephra layers from the distal records are based on archive specific age–depth models (Vakhrameeva *et al.* 2018, 2021; Leicher *et al.* 2021; Jordanova *et al.* 2022). Data for the LR04 are based on Lisiecki & Raymo (2005) with the MIS substages of Railsback *et al.* (2015). XRF data of the Lake Ohrid DEEP site from Wagner *et al.* (2019). The column ‘Synthesis of Italian volcanic activity’ combines all information. If robust correlations of equivalent eruptive events could be established and several ages were available, only the most reliable age is shown as discussed in the respective subchapter.



the WTT eruptive series. TF-70 (335.7 ± 3.0 ka) in turn is associated with an older unrecognized unit of the WTT series, which supports results by Quidelleur *et al.* (1997) and Rouchon *et al.* (2008), who suggested an age of 331.5 ± 2.0 ka for an undefined WTT unit. The volcanic origin of tephra layer TF-72 (340.8 ± 3.5 ka) is unclear, as it could correspond to an unknown pre-WTT eruption of the Roccamonfina volcano or to an unknown eruption from the Campanian volcanoes. Products of the Campanian Province are less frequently found within the Fucino succession, but volcanic activity of the Neapolitan volcanoes within the studied time interval is indicated by a proximal drill site (Trecase well, 300–370 ka, Brocchini *et al.* 2001) and in cryptotephra studies of sediment cores from the Ionian Sea and the Tenaghi Philippon records (Vakhrameeva *et al.* 2019, 2021).

The second cluster of tephra layers associated with Roccamonfina is interpreted as a closely spaced series of eruptions of the actual BLT eruptive series, including the major BLT eruption. Among the series of tephra found in Fucino, TF-77/–79 (351.7 ± 3.6 ka/ 355.1 ± 3.6 ka) may correspond to Plinian deposits predating the main eruptive BLT sequence (Luhr & Giannetti 1987). Tephra layer TF-75 with a $^{40}\text{Ar}/^{39}\text{Ar}$ age of 350.9 ± 3.0 ka represents the coarsest and thickest deposit of the series and thus probably represents the main caldera-forming eruptive phase. The overlying tephra layers TF-74e/–74d/–74a are interpreted as post-caldera eruptive pulses during the subsequent millennium. Although drilling disturbances biased the core quality of this interval and TF-74b/–c did not contain fresh glass, the different geochemical compositions of the individual tephra layers exclude reworking of older BLT deposits. This series of tephra layers suggests a more complex eruptive behaviour than that suggested by Rouchon *et al.* (2008), who interpreted the BLT as a single crisis event, and rather supports findings of Santello (2010), who described several subunits of the BLT, being deposited within a few thousand years.

The age of the oldest cluster of tephra layers TF-81/–82 is constrained by two new $^{40}\text{Ar}/^{39}\text{Ar}$ ages (362.7 ± 5.0 and 362.8 ± 3.2 ka) and has been tentatively associated with the BLT phase owing to their HKS character and temporal overlap with similar effusive products dated in the proximal area (369.0 ± 8.0 ka, La Frascara; 367.1 ± 9.0 ka, Galluccio; 357.1 ± 8.0 ka, Fontana–Radina; 355.1 ± 5.0 ka, Scipicciano; Rouchon *et al.* 2008). However, such pyroclastic deposits have not been described from the proximal area yet and the available data are too scarce to track the origin of TF-81/–82 at the present stage.

The eruptive activity of the Volsci Volcanic Field has not been recognized within the Fucino succession so far. Even if the ages of some of the recently re-dated eruptions (Boari *et al.* 2009b; Marra *et al.* 2021a) overlap with tephra layers of the F4–F5 record (TF-81–84, *c.* 365 ka),

the geochemical dataset available for the proximal VVD products does not support such a correlation.

The 313–366 ka Fucino tephra record in the framework of the Mediterranean tephrostratigraphy

The overall Mediterranean tephrostratigraphical framework of the time interval studied was previously only known from distal archives from the Ionian Sea (eight Italian tephra layers, Vakhrameeva *et al.* 2021), the terrestrial archives of Lake Ohrid (three Italian tephra layers, Leicher *et al.* 2019, 2021) and Tenaghi Philippon (nine Italian tephra layers, Vakhrameeva *et al.* 2018, 2019). The Fucino F4–F5 interval between 313 and 366 ka now stands as the most detailed and well-dated succession of 27 tephra layers from the Roman and Roccamonfina volcanoes (Fig. 8). An updated tephrostratigraphical framework combining distal archives and near-vent volcanic records is provided in Fig. 8. Both proximal and distal deposits indicate the frequent volcanic activity during the investigated time frame and thus highlight the great potential to find respective equivalents in other archives. However, correlations between different archives are still rare and only one correlation was tentatively proposed between the Fucino and ODP964 records (TF-74e/ODP964B 2H-5-67.5). Interestingly, the other numerous tephra layers associated with the Campanian Province found in the ODP964B and Tenaghi Philippon records could identified neither be in the Fucino nor in the Lake Ohrid successions and thus indicate the potential for cryptotephra analysis of these records. However, the absence of macroscopic evidence in these records may indicate a general shift in predominating wind directions during the course of eruptions with more south-easterly distribution of volcanic products. The proposed correlation of Fucino tephra layers TF-75/–77/–79 with the BAG tephra of the Loess–Palaeosol archives of the Danube basin represents a promising tie point for the alignment of different palaeoenvironmental archives on a larger regional scale. However, further geochemical analysis of the BAG and Fucino tephra layers is required to validate and specify the proposed correlation with a single layer, which based on the present data is most likely TF-77. Nevertheless, owing to the narrow age range (350–355 ka) of potential Fucino equivalents, the chronology of the loess sequences can already be improved (cf. Fig. 8), as previous correlations suggested a much older age for the BAG tephra (368 ka, Laag *et al.* 2021; *c.* 398 ka, Monaco *et al.* 2021; 368 ka, Jordanova *et al.* 2022).

Considering the climatostratigraphic position of tephra layers of the F4–F5 record based on Ti XRF data (Fig. 8), tephra layers TF-68/–69 to TF-72 deposited during the glacial termination III or the MIS 9/10 transition (337 ± 5 ka, Lisiecki & Raymo 2005). TF-68/–69 have been

directly dated and thus are very suitable as marker horizons for assessing spatial and temporal differences in changes of glacial to interglacial environmental conditions.

Conclusions

The volcanic origin of 27 tephra layers in the MIS 9/10 interval of the Fucino F4–F5 sediment succession was investigated based on their lithological, geochemical and chronological characteristics. Direct $^{40}\text{Ar}/^{39}\text{Ar}$ dating of six tephra layers set the basis for a Bayesian age–depth model for the interval 313–366 ka, which in turn provided modelled ages for the other tephra layers. The record provides the first tephrostratigraphical framework based on a continuous sediment succession of that time interval and at a suitable distance from the peri-Tyrrhenian volcanic centres for recording explosive eruptions of different intensity. Based on these results, the volcanic sources and, in some cases, the specific equivalent eruptions or eruptive phases of tephra layers have been identified. This information provides new insights into the eruptive history, mainly for major known eruptions of the Sabatini and Vulsini volcanic districts of the Roman Province and the Roccamonfina volcano. In addition, the resulting tephrostratigraphy of the Fucino succession represents a reference dataset for future correlations with specific (minor) eruptive events not yet conclusively identified in proximal settings. This significantly extends the available chronostratigraphical and compositional frame of Italian volcanism reconstructed from proximal areas. Moreover, the stratigraphically ordered succession also provided the possibility to reassess existing ages of eruptions with high temporal resolution.

Overall, the F4–F5 successions represents the richest tephra archive for this time interval of peri-Tyrrhenian volcanism and can thus be used as a reference record for a subsequent extension of the central Mediterranean tephrostratigraphical framework for this period. The large number of so far unidentified eruptive events and their similar geochemical patterns also indicate the need for (i) improving the proximal geochemical and geochronological data basis to reliably distinguish between closely spaced eruptions and validate proposed volcanic origins and (ii) a detailed geochemical investigation of distal ash layers detected in other archives to establish robust correlations.

Acknowledgements. – The Fucino project was founded by DFG (German Research Foundation) grant WA 2109/16. This article is a contribution to project ‘Fucino Tephrochronology Unites quaternary REcords (FUTURE)’, supported by the Italian Ministry of Education, University and Research (grant PRIN no. 20177TKBXZ_003; G. Zanchetta, coordinator). $^{40}\text{Ar}/^{39}\text{Ar}$ dating also received complementary contribution from the CNRS INSU-LEFE 2018-2020 action to S. Nomade. We also thank the editor, Jan A. Piotrowski, and the reviewers, Sabine Wulf and an anonymous reviewer, for valuable

comments and suggestions that helped to improve the manuscript. Open Access funding enabled and organized by Projekt DEAL.

Author contributions. – Conceptualization by NL, BG, BW, GZ; Data acquisition by NL, BG, AP, SN, LM, GM, PG, EP, GS; Data Curation by NL, AP, LM; Writing and visualization – original draft by NL; Writing and visualization – review and editing by all co-authors; Project administration and funding acquisition by BW, GZ, BG.

Data availability statement. – The geochemical EPMA-WDS data that support the findings of this study are openly available in Earthchem at <https://doi.org/10.26022/IEDA/112322>. The XRF data that support the findings of this study are available from the corresponding author upon reasonable request.

References

- Albert, P. G., Giaccio, B., Isaia, R., Costa, A., Niespolo, E. M., Nomade, S., Pereira, A., Renne, P. R., Hinchliffe, A., Mark, D. F., Brown, R. J. & Smith, V. C. 2019: Evidence for a large-magnitude eruption from Campi Flegrei caldera (Italy) at 29 ka. *Geology* 47, 595–599.
- Albert, P. G., Tomlinson, E. L., Smith, V. C., Di Roberto, A., Todman, A., Rosi, M., Marani, M., Müller, W. & Menzies, M. A. 2012: Marine-continental tephra correlations: volcanic glass geochemistry from the Marsili Basin and the Aeolian Islands, southern Tyrrhenian Sea, Italy. *Journal of Volcanology and Geothermal Research* 229, 74–94.
- Amato, V., Aucelli, P. P. C., Cesarano, M., Jicha, B., Lebreton, V., Orain, R., Pappone, G., Petrosino, P. & Ermolli, E. R. 2014: Quaternary evolution of the largest intermontane basin of the Molise Apennine (Central-Southern Italy). *Rendiconti Lincei* 25, 197–216.
- Balbas, A., Koppers, A. A. P., Kent, D. V., Konrad, K. & Clark, P. U. 2016: Identification of the short-lived Santa Rosa geomagnetic excursion in lavas on Floreana Island (Galapagos) by $^{40}\text{Ar}/^{39}\text{Ar}$ geochronology. *Geology* 44, 359–362.
- Belkin, H. E., Rolandi, G., Jackson, J. C., Cannatelli, C., Doherty, A. L., Petrosino, P. & De Vivo, B. 2016: Mineralogy and geochemistry of the older (>40 ka) ignimbrites on the Campanian plain, southern Italy. *Journal of Volcanology and Geothermal Research* 323, 1–18.
- Blaauw, M. & Christen, J. A. 2011: Flexible paleoclimate age–depth models using an autoregressive gamma process. *Bayesian Analysis* 6, 457–474.
- Blockley, S. P. E., Bourne, A. J., Brauer, A., Davies, S. M., Hardiman, M., Harding, P. R., Lane, C. S., MacLeod, A., Matthews, I. P., Pyne-O'Donnell, S. D. F., Rasmussen, S. O., Wulf, S. & Zanchetta, G. 2014: Tephrochronology and the extended intimate (integration of ice-core, marine and terrestrial records) event stratigraphy 8–128 ka b2k. *Quaternary Science Reviews* 106, 88–100.
- Boari, E., Avanzinelli, R., Melluso, L., Giordano, G., Mattei, M., De Benedetti, A. A., Morra, V. & Conticelli, S. 2009a: Isotope geochemistry (Sr–Nd–Pb) and petrogenesis of leucite-bearing volcanic rocks from ‘Colli Albani’ volcano, Roman Magmatic Province, Central Italy: inferences on volcano evolution and magma genesis. *Bulletin of Volcanology* 71, 977–1005.
- Boari, E., Tommasini, S., Laurenzi, M. A. & Conticelli, S. 2009b: Transition from ultrapotassic Kamafugitic to sub-alkaline magmas: Sr, Nd, and Pb isotope, trace element and $^{40}\text{Ar}/^{39}\text{Ar}$ age data from the middle Latin Valley volcanic field, Roman Magmatic Province, Central Italy. *Journal of Petrology* 50, 1327–1357.
- Bourne, A. J., Albert, P. G., Matthews, I. P., Trincardi, F., Wulf, S., Asioli, A., Blockley, S. P. E., Keller, J. & Lowe, J. J. 2015: Tephrochronology of core PRAD 1-2 from the Adriatic Sea: insights into Italian explosive volcanism for the period 200–80 ka. *Quaternary Science Reviews* 116, 28–43.
- Brauer, A., Wulf, S., Mangili, C., Appelt, O. & Moscardiello, A. 2007a: Reply: tephrochronological dating of varved interglacial lake deposits from Piànico-Sèllere (southern Alps, Italy) to around 400 ka. *Journal of Quaternary Science* 22, 415–418.
- Brauer, A., Wulf, S., Mangili, C. & Moscardiello, A. 2007b: Tephrochronological dating of varved interglacial lake deposits

- from Piànico-Sèllere (southern Alps, Italy) to around 400 ka. *Journal of Quaternary Science* 22, 85–96.
- Brocchini, D., Principe, C., Castradori, D., Laurenzi, M. A. & Gorla, L. 2001: Quaternary evolution of the southern sector of the Campanian plain and early Somma-Vesuvius activity: insights from the Trecase 1 well. *Mineralogy and Petrology* 73, 67–91.
- Calanchi, N. & Dinelli, E. 2008: Tephrostratigraphy of the last 170 ka in sedimentary successions from the Adriatic Sea. *Journal of Volcanology and Geothermal Research* 177, 81–95.
- Cardello, G. L., Consorti, L., Palladino, D. M., Carminati, E., Carlini, M. & Dogliani, C. 2020: Tectonically controlled carbonate-seated maar-diatreme volcanoes: the case of the Volsci volcanic field, Central Italy. *Journal of Geodynamics* 139, 101763, <https://doi.org/10.1016/j.jog.2020.101763>.
- Cavinato, G. P., Carusi, C., Dall'Asta, M., Miccadei, E. & Piacentini, T. 2002: Sedimentary and tectonic evolution of Plio-Pleistocene alluvial and lacustrine deposits of Fucino Basin (Central Italy). *Sedimentary Geology* 148, 29–59.
- Cox, S. E., Hemming, S. R. & Tootell, D. 2020: The Isotopx NGX and ATONA faraday amplifiers. *Geochronology* 2, 231–243.
- Cross, J. K., Tomlinson, E. L., Giordano, G., Smith, V. C., De Benedetti, A. A., Roberge, J., Manning, C. J., Wulf, S. & Menzies, M. A. 2014: High level triggers for explosive mafic volcanism: Albano maar, Italy. *Lithos* 190–191, 137–153.
- D'Agostino, N., Jackson, J. A., Dramis, F. & Funicello, R. 2001: Interactions between mantle upwelling, drainage evolution and active normal faulting: an example from the central Apennines (Italy). *Geophysical Journal International* 147, 475–497.
- Del Carlo, P., Smedile, A., Petrelli, M. & Di Roberto, A. 2020: Evidence for an unknown explosive eruption of Mt. Etna volcano (Italy) during the late glacial. *Journal of Volcanology and Geothermal Research* 402, 106992, <https://doi.org/10.1016/j.jvolgeores.2020.106992>.
- Di Roberto, A., Smedile, A., Del Carlo, P., De Martini, P. M., Iorio, M., Petrelli, M., Pantosti, D., Pinzi, S. & Todrani, A. 2018: Tephra and cryptotephra in a ~ 60,000-year-old lacustrine sequence from the Fucino Basin: new insights into the major explosive events in Italy. *Bulletin of Volcanology* 80, 20, <https://doi.org/10.1007/s00445-018-1200-x>.
- Forni, F., Lucchi, F., Peccerillo, A., Tranne, C. A., Rossi, P. L. & Frezzotti, M. L. 2013: Stratigraphy and geological evolution of the Lipari volcanic complex (central aeolian archipelago). In Lucchi, F., Peccerillo, A., Keller, J., Tranne, C. A. & Rossi, P. L. (eds.): *The Aeolian Islands Volcanoes*, 213–279. Geological Society, London.
- Freda, C., Gaeta, M., Karner, D. B., Marra, F., Renne, P. R., Taddeucci, J., Scarlato, P., Christensen, J. N. & Dallai, L. 2006: Eruptive history and petrologic evolution of the Albano multiple maar (Alban Hills, Central Italy). *Bulletin of Volcanology* 68, 567–591.
- Gaeta, M., Freda, C., Christensen, J. N., Dallai, L., Marra, F., Karner, D. B. & Scarlato, P. 2006: Time-dependent geochemistry of clinopyroxene from the Alban Hills (Central Italy): clues to the source and evolution of ultrapotassic magmas. *Lithos* 86, 330–346.
- Gaeta, M., Freda, C., Marra, F., Arienzo, I., Gozzi, F., Jicha, B. & Di Rocco, T. 2016: Paleozoic metasomatism at the origin of Mediterranean ultrapotassic magmas: constraints from time-dependent geochemistry of Colli Albani volcanic products (Central Italy). *Lithos* 244, 151–164.
- Gaeta, M., Freda, C., Marra, F., Di Rocco, T., Gozzi, F., Arienzo, I., Giaccio, B. & Scarlato, P. 2011: Petrology of the most recent ultrapotassic magmas from the Roman Province (Central Italy). *Lithos* 127, 298–308.
- Galadini, F. & Galli, P. 2000: Active tectonics in the central Apennines (Italy) – input data for seismic Hazard assessment. *Natural Hazards* 22, 225–268.
- Galli, P., Giaccio, B., Messina, P., Peronace, E., Amato, V., Naso, G., Nomade, S., Pereira, A., Piscitelli, S., Bellanova, J., Billi, A., Blamart, D., Galderisi, A., Giocoli, A., Stabile, T. & Thil, F. 2017: Middle to late Pleistocene activity of the northern Matese fault system (southern Apennines, Italy). *Tectonophysics* 699, 61–81.
- Giaccio, B., Arienzo, I., Sottili, G., Castorina, F., Gaeta, M., Nomade, S., Galli, P. & Messina, P. 2013b: Isotopic (Sr-Nd) and major element fingerprinting of distal tephra: an application to the middle-late Pleistocene markers from the Colli Albani volcano, Central Italy. *Quaternary Science Reviews* 67, 190–206.
- Giaccio, B., Castorina, F., Nomade, S., Scardia, G., Voltaggio, M. & Sagnotti, L. 2013a: Revised chronology of the Sulmona lacustrine succession, Central Italy. *Journal of Quaternary Science* 28, 545–551.
- Giaccio, B., Galli, P., Messina, P., Peronace, E., Scardia, G., Sottili, G., Sposato, A., Chiarini, E., Jicha, B. & Silvestri, S. 2012: Fault and basin depocentre migration over the last 2 ma in the L'Aquila 2009 earthquake region, central Italian Apennines. *Quaternary Science Reviews* 56, 69–88.
- Giaccio, B., Galli, P., Peronace, E., Arienzo, I., Nomade, S., Cavinato, G. P., Mancini, M., Messina, P. & Sottili, G. 2014: A 560–440 ka tephra record from the Mercure Basin, southern Italy: volcanological and tephrostratigraphic implications. *Journal of Quaternary Science* 29, 232–248.
- Giaccio, B., Hajdas, I., Isaia, R., Deino, A. & Nomade, S. 2017b: High-precision ^{14}C and $^{40}\text{Ar}/^{39}\text{Ar}$ dating of the Campanian ignimbrite (Y-5) reconciles the time-scales of climatic-cultural processes at 40 ka. *Scientific Reports* 7, 45940, <https://doi.org/10.1038/srep45940>.
- Giaccio, B., Leicher, N., Mannella, G., Monaco, L., Regattieri, E., Wagner, B., Zanchetta, G., Gaeta, M., Marra, F., Nomade, S., Palladino, D. M., Pereira, A., Scheidt, S., Sottili, G., Wonik, T., Wulf, S., Zeeden, C., Ariztegui, D., Cavinato, G. P., Dean, J. R., Florindo, F., Leng, M. J., Macri, P., Niespolo, E., Renne, P. R., Rolf, C., Sadori, L., Thomas, C. & Tzedakis, P. C. 2019: Extending the tephra and palaeoenvironmental record of the Central Mediterranean back to 430 ka: a new core from Fucino Basin, Central Italy. *Quaternary Science Reviews* 225, 106003, <https://doi.org/10.1016/j.quascirev.2019.106003>.
- Giaccio, B., Marino, G., Marra, F., Monaco, L., Pereira, A., Zanchetta, G., Gaeta, M., Leicher, N., Nomade, S., Palladino, D. M., Sottili, G., Guillou, H. & Scao, V. 2021: Tephrochronological constraints on the timing and nature of sea-level change prior to and during glacial termination V. *Quaternary Science Reviews* 263, 106976, <https://doi.org/10.1016/j.quascirev.2021.106976>.
- Giaccio, B., Niespolo, E. M., Pereira, A., Nomade, S., Renne, P. R., Albert, P. G., Arienzo, I., Regattieri, E., Wagner, B., Zanchetta, G., Gaeta, M., Galli, P., Mannella, G., Peronace, E., Sottili, G., Florindo, F., Leicher, N., Marra, F. & Tomlinson, E. L. 2017a: First integrated tephrochronological record for the last ~ 190 kyr from the Fucino quaternary lacustrine succession, Central Italy. *Quaternary Science Reviews* 158, 211–234.
- Giaccio, B., Regattieri, E., Zanchetta, G., Nomade, S., Renne, P. R., Sprain, C. J., Drysdale, R. N., Tzedakis, P. C., Messina, P., Scardia, G., Sposato, A. & Bassinot, F. 2015a: Duration and dynamics of the best orbital analogue to the present interglacial. *Geology* 43, 603–606.
- Giaccio, B., Regattieri, E., Zanchetta, G., Wagner, B., Galli, P., Mannella, G., Niespolo, E., Peronace, E., Renne, P. R., Nomade, S., Cavinato, G. P., Messina, P., Sposato, A., Boschi, C., Florindo, F., Marra, F. & Sadori, L. 2015b: A key continental archive for the last 2 ma of climatic history of the Central Mediterranean region: a pilot drilling in the Fucino Basin, Central Italy. *Scientific Drilling* 20, 13–19.
- Giannetti, B. 2001: Origin of the calderas and evolution of Roccamonfina volcano (Roman region, Italy). *Journal of Volcanology and Geothermal Research* 106, 301–319.
- Giannetti, B. & De Casa, G. 2000: Stratigraphy, chronology, and sedimentology of ignimbrites from the white trachytic tuff, Roccamonfina volcano, Italy. *Journal of Volcanology and Geothermal Research* 96, 243–295.
- Giordano, G., De Benedetti, A., Diana, A., Diano, G., Esposito, A., Fabbri, M., Gaudio, F., Marasco, F., Mazzini, I. & Miceli, M. 2010: Stratigraphy, volcano tectonics and evolution of the Colli Albani volcanic field. In Funicello, R. & Giordano, G. (eds.): *The Colli Albani Volcano*, 43–97. Geological Society of London, London.
- Insinga, D. D., Tamburrino, S., Lirer, F., Vezzoli, L., Barra, M., De Lange, G. J., Tiepolo, M., Vallefucio, M., Mazzola, S. & Sprovieri, M. 2014: Tephrochronology of the astronomically-tuned KC01B deep-sea core, Ionian Sea: insights into the explosive activity of the Central Mediterranean area during the last 200 ka. *Quaternary Science Reviews* 85, 63–84.

- Jordanova, D., Laag, C., Jordanova, N., Lagroix, F., Georgieva, B., Ishlyanski, D. & Guyodo, Y. 2022: A detailed magnetic record of Pleistocene climate and distal ash dispersal during the last 800 kyrs—the Suhia Kladenetz quarry loess-paleosol sequence near Pleven (Bulgaria). *Global and Planetary Change* 214, 103840, <https://doi.org/10.1016/j.gloplacha.2022.103840>.
- Karner, D. B., Marra, F. & Renne, P. R. 2001: The history of the Monti Sabatini and Alban Hills volcanoes: groundwork for assessing volcanic-tectonic hazards for Rome. *Journal of Volcanology and Geothermal Research* 107, 185–219.
- Keller, J., Ryan, W. B. F., Ninkovich, D. & Altherr, R. 1978: Explosive volcanic activity in the Mediterranean over the past 200,000 yr as recorded in deep-sea sediments. *Geological Society of America Bulletin* 89, 591–604.
- Koppers, A. A. 2002: ArArCALC—software for $^{40}\text{Ar}/^{39}\text{Ar}$ age calculations. *Computers & Geosciences* 28, 605–619.
- Laag, C., Hambach, U., Zeeden, C., Lagroix, F., Guyodo, Y., Veres, D., Jovanovic, M. & Markovic, S. B. 2021: A detailed paleoclimate proxy record for the middle Danube Basin over the last 430 kyr: a rock magnetic and colorimetric study of the Zemun loess-paleosol sequence. *Frontiers in Earth Science* 9, 600086, <https://doi.org/10.3389/feart.2021.600086>.
- Lanari, R., Faccenna, C., Benedetti, L., Sembroni, A., Bellier, O., Menichelli, I., Primerano, P. & Molin, P. 2021: Formation and persistence of extensional internally drained basins: the case of the Fucino Basin (central Apennines, Italy). *Tectonics* 40, e2020TC006442, <https://doi.org/10.1029/2020TC006442>.
- Lane, C. S., Lowe, D. J., Blockley, S. P. E., Suzuki, T. & Smith, V. C. 2017: Advancing tephrochronology as a global dating tool: applications in volcanology, archaeology, and palaeoclimatic research. *Quaternary Geochronology* 40, 1–7.
- Le Bas, M. J. L., Maitre, R. W. L., Streckeisen, A. & Zanettin, B. 1986: A chemical classification of volcanic rocks based on the Total alkali-silica diagram. *Journal of Petrology* 27, 745–750.
- Lee, J. Y., Marti, K., Severinghaus, J. P., Kawamura, K., Yoo, H. S., Lee, J. B. & Kim, J. S. 2006: A redetermination of the isotopic abundances of atmospheric Ar. *Geochimica et Cosmochimica Acta* 70, 4507–4512.
- Leicher, N. 2021: *EPMA-WDS settings for glass at University of Cologne - v1, version 1.0*. Interdisciplinary Earth Data Alliance (IEDA). <https://doi.org/10.26022/IEDA/111986>.
- Leicher, N. & Giaccio, B. 2021: *EPMA-WDS settings for glass at IGAG-CNR- v1, version 1.0*. Interdisciplinary Earth Data Alliance (IEDA). <https://doi.org/10.26022/IEDA/111987>.
- Leicher, N., Giaccio, B., Zanchetta, G., Sulpizio, R., Albert, P. G., Tomlinson, E. L., Lagos, M., Francke, A. & Wagner, B. 2021: Lake Ohrid's tephrochronological dataset reveals 1.36 ma of Mediterranean explosive volcanic activity. *Scientific Data* 8, 231, <https://doi.org/10.1038/s41597-021-01013-7>.
- Leicher, N., Giaccio, B., Zanchetta, G., Wagner, B., Francke, A., Palladino, D. M., Sulpizio, R., Albert, P. G. & Tomlinson, E. L. 2019: Central Mediterranean explosive volcanism and tephrochronology during the last 630 ka based on the sediment record from Lake Ohrid. *Quaternary Science Reviews* 226, 106021, <https://doi.org/10.1016/j.quascirev.2019.106021>.
- Leicher, N., Monaco, L., Giaccio, B., Sottili, G., Galli, P. & Peronace, E. 2023: Glass geochemical composition of tephra layers of the interval 366–313 ka from the Fucino record and proximal equivalents, version 1.0. *Interdisciplinary Earth Data Alliance (IEDA)*, <https://doi.org/10.26022/IEDA/112322>.
- Lisiecki, L. E. & Raymo, M. E. 2005: A Pliocene-Pleistocene stack of 57 globally distributed benthic $\delta^{18}\text{O}$ records. *Paleoceanography* 20, PA1003, <https://doi.org/10.1029/2004PA001071>.
- Ludwig, K. R. 2009: Isoplot 3.70: a geochronological toolkit for Microsoft excel. *Berkeley Geochronology Center Special Publication* 4, 1–76.
- Luhr, J. F. & Giannetti, B. 1987: The Brown leucitic tuff of Roccamonfina volcano (Roman region, Italy). *Contributions to Mineralogy and Petrology* 95, 420–436.
- Mahood, G. A. & Hildreth, W. 1986: Geology of the peralkaline volcano at Pantelleria, strait of Sicily. *Bulletin of Volcanology* 48, 143–172.
- Mannella, G., Giaccio, B., Zanchetta, G., Regattieri, E., Niespolo, E. M., Pereira, A., Renne, P. R., Nomade, S., Leicher, N., Perchiazzi, N. & Wagner, B. 2019: Palaeoenvironmental and palaeohydrological variability of mountain areas in the Central Mediterranean region: a 190 ka-long chronicle from the independently dated Fucino palaeolake record (Central Italy). *Quaternary Science Reviews* 210, 190–210.
- Marra, F., Cardello, G. L., Gaeta, M., Jicha, B. R., Montone, P., Niespolo, E. M., Nomade, S., Palladino, D. M., Pereira, A., De Luca, G., Florindo, F., Frepoli, A., Renne, P. R. & Sottili, G. 2021a: The Volsi volcanic field (Central Italy): eruptive history, magma system and implications on continental subduction processes. *International Journal of Earth Sciences* 110, 689–718.
- Marra, F., Castellano, C., Cucci, L., Florindo, F., Gaeta, M., Jicha, B. R., Palladino, D. M., Sottili, G., Tertulliani, A. & Tolomei, C. 2020a: Monti Sabatini and Colli Albani: the dormant twin volcanoes at the gates of Rome. *Scientific Reports* 10, 8666, <https://doi.org/10.1038/s41598-020-65394-2>.
- Marra, F., Costantini, L., Di Buduo, G. M., Florindo, F., Jicha, B. R., Monaco, L., Palladino, D. M. & Sottili, G. 2019: Combined glacio-eustatic forcing and volcano-tectonic uplift: geomorphological and geochronological constraints on the Tiber River terraces in the eastern Vulsini Volcanic District (Central Italy). *Global and Planetary Change* 182, 103009, <https://doi.org/10.1016/j.gloplacha.2019.103009>.
- Marra, F., Deocampo, D., Jackson, M. D. & Ventura, G. 2011: The Alban Hills and Monti Sabatini volcanic products used in ancient Roman masonry (Italy): an integrated stratigraphic, archaeological, environmental and geochemical approach. *Earth-Science Reviews* 108, 115–136.
- Marra, F., Freda, C., Scarlato, P., Taddeucci, J., Karner, D. B., Renne, P. R., Gaeta, M., Palladino, D. M., Trigila, R. & Cavarretta, G. 2003: Post-caldera activity in the Alban Hills volcanic district (Italy): $^{40}\text{Ar}/^{39}\text{Ar}$ geochronology and insights into magma evolution. *Bulletin of Volcanology* 65, 227–247.
- Marra, F., Gaeta, M., Giaccio, B., Jicha, B. R., Palladino, D. M., Polcaro, M., Sottili, G., Taddeucci, J., Florindo, F. & Stramondo, S. 2016b: Assessing the volcanic hazard for Rome: $^{40}\text{Ar}/^{39}\text{Ar}$ and InSAR constraints on the most recent eruptive activity and present-day uplift at Colli Albani Volcanic District. *Geophysical Research Letters* 43, 6898–6906.
- Marra, F., Jicha, B., Palladino, D. M., Gaeta, M., Costantini, L. & Di Buduo, G. M. 2020b: $^{40}\text{Ar}/^{39}\text{Ar}$ single crystal dates from pyroclastic deposits provide a detailed record of the 590–240 ka eruptive period at the Vulsini Volcanic District (Central Italy). *Journal of Volcanology and Geothermal Research* 398, 106904, <https://doi.org/10.1016/j.jvolgeores.2020.106904>.
- Marra, F., Karner, D. B., Freda, C., Gaeta, M. & Renne, P. 2009: Large mafic eruptions at Alban Hills Volcanic District (Central Italy): Chronostratigraphy, petrography and eruptive behavior. *Journal of Volcanology and Geothermal Research* 179, 217–232.
- Marra, F., Pereira, A., Jicha, B., Nomade, S., Biddittu, I., Florindo, F., Muttoni, G., Niespolo, E., Renne, P. & Scao, V. 2021b: Terrestrial records of glacial terminations V and IV and insights on deglacial mechanisms. *Climate of the Past Discussions* 2021, 1–32.
- Marra, F., Rohling, E. J., Florindo, F., Jicha, B., Nomade, S., Pereira, A. & Renne, P. R. 2016a: Independent $^{40}\text{Ar}/^{39}\text{Ar}$ and ^{14}C age constraints on the last five glacial terminations from the aggradational successions of the Tiber River, Rome (Italy). *Earth and Planetary Science Letters* 449, 105–117.
- Marra, F., Sottili, G., Gaeta, M., Giaccio, B., Jicha, B., Masotta, M., Palladino, D. M. & Deocampo, D. M. 2014: Major explosive activity in the Monti Sabatini Volcanic District (Central Italy) over the 800–390 ka interval: geochronological-geochemical overview and tephrostratigraphic implications. *Quaternary Science Reviews* 94, 74–101.
- Monaco, L., Leicher, N., Palladino, D. M., Arienzo, I., Marra, F., Petrelli, M., Nomade, S., Pereira, A., Sottili, G., Conticelli, S., D'Antonio, M., Fabbriozzi, A., Jicha, B. R., Mannella, G., Petrosino, P., Regattieri, E., Tzedakis, P. C., Wagner, B., Zanchetta, G. & Giaccio, B. 2022b: The Fucino 250–170 ka tephra record: new insights on peri-Tyrrhenian explosive volcanism, central mediterranean tephrochronology, and timing of the MIS 8-6 climate variability. *Quaternary Science Reviews* 296, 107797, <https://doi.org/10.1016/j.quascirev.2022.107797>.

- Monaco, L., Palladino, D. M., Albert, P. G., Arienzo, I., Conticelli, S., Di Vito, M., Fabbriozzi, A., D'Antonio, M., Isaia, R., Manning, C. J., Nomade, S., Pereira, A., Petrosino, P., Sottili, G., Sulpizio, R., Zanchetta, G. & Giaccio, B. 2022a: Linking the Mediterranean MIS 5 tephra markers to Campi Flegrei (southern Italy) 109–92 ka explosive activity and refining the chronology of MIS 5c-d millennial-scale climate variability. *Global and Planetary Change* 211, 103785, <https://doi.org/10.1016/j.gloplacha.2022.103785>.
- Monaco, L., Palladino, D. M., Gaeta, M., Marra, F., Sottili, G., Leicher, N., Mannella, G., Nomade, S., Pereira, A., Regattieri, E., Wagner, B., Zanchetta, G., Albert, P. G., Arienzo, I., D'Antonio, M., Petrosino, P., Manning, C. J. & Giaccio, B. 2021: Mediterranean tephrostratigraphy and peri-Tyrrhenian explosive activity reevaluated in light of the 430–365 ka record from Fucino Basin (Central Italy). *Earth-Science Reviews* 220, 103706, <https://doi.org/10.1016/j.earscirev.2021.103706>.
- Mondati, G., Spadi, M., Gliozzi, E., Cosentino, D., Cifelli, F., Cavinato, G. P., Tallini, M. & Mattei, M. 2021: The tectono-stratigraphic evolution of the Fucino Basin (central Apennines, Italy): new insights from the geological mapping of its north-eastern margin. *Journal of Maps* 17, 87–100.
- Munno, R. & Petrosino, P. 2007: The late quaternary tephrostratigraphical record of the san Gregorio Magno basin (southern Italy). *Journal of Quaternary Science* 22, 247–266.
- Nappi, G., Capaccioni, B., Mattioli, M., Mancini, E. & Valentini, L. 1994: Plinian fall deposits from Vulsini Volcanic District (Central Italy). *Bulletin of Volcanology* 56, 502–515.
- Nappi, G., Renzulli, A., Santi, P. & Gillot, P. Y. 1995: Geological evolution and geochronology of the Vulsini volcanic district (Central Italy). *Bollettino della Societa Geologica Italiana* 114, 599–613.
- Narcisi, B. & Vezzoli, L. 1999: Quaternary stratigraphy of distal tephra layers in the Mediterranean - an overview. *Global and Planetary Change* 21, 31–50.
- Niespolo, E. M., Rutte, D., Deino, A. L. & Renne, P. R. 2017: Intercalibration and age of the Alder Creek sanidine $^{40}\text{Ar}/^{39}\text{Ar}$ standard. *Quaternary Geochronology* 39, 205–213.
- Nomade, S., Muttoni, G., Guillou, H., Robin, E. & Scardia, G. 2011: First $^{40}\text{Ar}/^{39}\text{Ar}$ age of the Ceprano man (Central Italy). *Quaternary Geochronology* 6, 453–457.
- Palladino, D. M., Gaeta, M., Giaccio, B. & Sottili, G. 2014: On the anatomy of magma chamber and caldera collapse: the example of trachy-phonolitic explosive eruptions of the Roman Province (Central Italy). *Journal of Volcanology and Geothermal Research* 281, 12–26.
- Palladino, D. M., Simei, S., Sottili, G. & Trigila, R. 2010: Integrated approach for the reconstruction of stratigraphy and geology of quaternary volcanic terrains: an application to the Vulsini volcanoes (Central Italy). *Geological Society of America Special Papers* 464, 63–84.
- Patacca, E., Scandone, P., Di Luzio, E., Cavinato, G. P. & Parotto, M. 2008: Structural architecture of the central Apennines: interpretation of the CROP 11 seismic profile from the Adriatic coast to the orographic divide. *Tectonics* 27, TC3006, <https://doi.org/10.1029/2005TC001917>.
- Paterne, M., Guichard, F., Duplessy, J. C., Siani, G., Sulpizio, R. & Labeyrie, J. 2008: A 90,000–200,000 yrs marine tephra record of Italian volcanic activity in the Central Mediterranean Sea. *Journal of Volcanology and Geothermal Research* 177, 187–196.
- Paterne, M., Guichard, F. & Labeyrie, J. 1988: Explosive activity of the south Italian volcanoes during the past 80,000 years as determined by marine tephrochronology. *Journal of Volcanology and Geothermal Research* 34, 153–172.
- Peccerillo, A. & Frezzotti, M. L. 2015: Magmatism, mantle evolution and geodynamics at the converging plate margins of Italy. *Journal of the Geological Society* 172, 407–427.
- Pereira, A., Monaco, L., Marra, F., Nomade, S., Gaeta, M., Leicher, N., Palladino, D. M., Sottili, G., Guillou, H., Scao, V. & Giaccio, B. 2020: Tephrochronology of the Central Mediterranean MIS 11c interglacial (~425–395 ka): new constraints from the Vico volcano and Tiber delta, Central Italy. *Quaternary Science Reviews* 243, 106470, <https://doi.org/10.1016/j.quascirev.2020.106470>.
- Pereira, A., Nomade, S., Falguères, C., Bahain, J.-J., Tombret, O., Garcia, T., Voinchet, P., Bulgarelli, G.-M. & Anzidei, A.-P. 2017: $^{40}\text{Ar}/^{39}\text{Ar}$ and ESR/U-series data for the La Polledrara di Cecanibbio archaeological site (Lazio, Italy). *Journal of Archaeological Science: Reports* 15, 20–29.
- Pereira, A., Nomade, S., Moncel, M. H., Voinchet, P., Bahain, J. J., Biddittu, I., Falgueres, C., Giaccio, B., Manzi, G., Parenti, F., Scardia, G., Scao, V., Sottili, G. & Vietti, A. 2018: Integrated geochronology of Acheulian sites from the southern Latium (central Italy): Insights on human-environment interaction and the technological innovations during the MIS 11-MIS 10 period. *Quaternary Science Reviews* 187, 112–129.
- Pereira, A., Nomade, S., Shao, Q., Bahain, J.-J., Arzarello, M., Douville, E., Falguères, C., Frank, N., Garcia, T., Lembo, G., Muttillio, B., Scao, V. & Peretto, C. 2016: $^{40}\text{Ar}/^{39}\text{Ar}$ and ESR/U-series dates for Guado san Nicola, middle Pleistocene key site at the lower/middle Palaeolithic transition in Italy. *Quaternary Geochronology* 36, 67–75.
- Perini, G. & Conticelli, S. 2002: Crystallization conditions of leucite-bearing magmas and their implications on the magmatological evolution of ultrapotassic magmas: the Vico volcano, Central Italy. *Mineralogy and Petrology* 74, 253–276.
- Perini, G., Francalanci, L., Davidson, J. P. & Conticelli, S. 2004: Evolution and genesis of magmas from Vico volcano, Central Italy: multiple differentiation pathways and variable parental magmas. *Journal of Petrology* 45, 139–182.
- Petrosino, P., Arienzo, I., Mazzeo, F. C., Natale, J., Petrelli, M., Milia, A., Perugini, D. & D'Antonio, M. 2019: The san Gregorio Magno lacustrine basin (Campania, southern Italy): improved characterization of the tephrostratigraphic markers based on trace elements and isotopic data. *Journal of Quaternary Science* 34, 393–404.
- Petrosino, P., Jicha, B. R., Mazzeo, F. C., Ciaranfi, N., Girone, A., Maiorano, P. & Marino, M. 2015: The Montalbano Jonico marine succession: an archive for distal tephra layers at the early–middle Pleistocene boundary in southern Italy. *Quaternary International* 383, 89–103.
- Petrosino, P., Jicha, B. R., Mazzeo, F. C. & Russo Ermolli, E. 2014: A high resolution tephrochronological record of MIS 14–12 in the southern Apennines (Acerno Basin, Italy). *Journal of Volcanology and Geothermal Research* 274, 34–50.
- Pinti, D. L., Quidelleur, X., Chiesa, S., Ravazzi, C. & Gillot, P.-Y. 2001: K–Ar dating of an early middle Pleistocene distal tephra in the interglacial varved succession of Pianico-Sèllere (southern Alps, Italy). *Earth and Planetary Science Letters* 188, 1–7.
- Pinti, D. L., Rouchon, V., Quidelleur, X., Gillot, P.-Y., Chiesa, S. & Ravazzi, C. 2007: Comment: tephrochronological dating of varved interglacial lake deposits from Pianico-Sèllere (southern Alps, Italy) to around 400 ka. *Journal of Quaternary Science* 22, 411–414.
- Poulet, A., Horvath, E., Gabris, G. & Juvigné, E. 1999: The bag tephra, a widespread tephrochronological marker in middle Europe: chemical and mineralogical investigations. *Bulletin of Volcanology* 61, 265–272.
- Quidelleur, X., Gillot, P. Y., Grove, M., Harrison, T. M. & Deino, A. 1997: The white trachytic tuff sanidine: a potential age standard for $^{40}\text{Ar}/^{39}\text{Ar}$ dating of Pleistocene-Pliocene samples. *Terra Cognita* 9, p. 69.
- R Core Team 2022: *R: A Language and Environment for Statistical Computing*. R Foundation for Statistical Computing, Vienna, Austria.
- Railsback, L. B., Gibbard, P. L., Head, M. J., Voarintsoa, N. R. G. & Toucanne, S. 2015: An optimized scheme of lettered marine isotope substages for the last 1.0 million years, and the climatostratigraphic nature of isotope stages and substages. *Quaternary Science Reviews* 111, 94–106.
- Regattieri, E., Giaccio, B., Zanchetta, G., Drysdale, R. N., Galli, P., Nomade, S., Peronace, E. & Wulf, S. 2015: Hydrological variability over the Apennines during the early last glacial precession minimum, as revealed by a stable isotope record from Sulmona basin, Central Italy. *Journal of Quaternary Science* 30, 19–31.
- Renne, P. R., Balco, G., Ludwig, K. R., Mundil, R. & Min, K. 2011: Response to the comment by WH Schwarz et al. on 'joint determination of ^{40}K decay constants and $^{40}\text{Ar}/^{40}\text{K}$ for the fish canyon sanidine standard, and improved accuracy for $^{40}\text{Ar}/^{39}\text{Ar}$ geochronology' by PR Renne et al. (2010). *Geochimica et Cosmochimica Acta* 75, 5097–5100.

- Rolandi, G., Bellucci, F., Heizler, M. T., Belkin, H. E. & De Vivo, B. 2003: Tectonic controls on the genesis of ignimbrites from the Campanian volcanic zone, southern Italy. *Mineralogy and Petrology* 79, 3–31.
- Rouchon, V., Gillot, P. Y., Quidelleur, X., Chiesa, S. & Floris, B. 2008: Temporal evolution of the Roccamonfina volcanic complex (Pleistocene), Central Italy. *Journal of Volcanology and Geothermal Research* 177, 500–514.
- Rouilleau, E., Pinti, D. L., Rouchon, V., Quidelleur, X. & Gillot, P.-Y. 2009: Tephro-chronostratigraphy of the lacustrine interglacial record of Piànico, Italian southern Alps: identifying the volcanic sources using radiogenic isotopes and trace elements. *Quaternary International* 204, 31–43.
- Ryan, W. B. F., Carbotte, S. M., Coplan, J. O., O'Hara, S., Melkonian, A., Arko, R., Weissel, R. A., Ferrini, V., Goodwillie, A., Nitsche, F., Bonczkowski, J. & Zemsky, R. 2009: Global multi-resolution topography synthesis. *Geochemistry Geophysics Geosystems* 10, 1525–2027.
- Santello, L. 2010: *Analysis of a Trampled Formation: The Brown Leucitic Tuff (Roccamonfina Volcano, Southern Italy)*. Ph.D. thesis, University of Padova, 154 pp.
- Scaillet, S., Vita-Scaillet, G. & Guillou, H. 2008: Oldest human footprints dated by Ar/Ar. *Earth and Planetary Science Letters* 275, 320–325.
- Scardia, G. & Muttoni, G. 2009: Paleomagnetic investigations on the Pleistocene lacustrine sequence of Piànico-Sèllere (northern Italy). *Quaternary International* 204, 44–53.
- Sottili, G., Arienzo, I., Castorina, F., Gaeta, M., Giaccio, B., Marra, F. & Palladino, D. M. 2019: Time-dependent Sr and Nd isotope variations during the evolution of the ultrapotassic Sabatini Volcanic District (Roman province, Central Italy). *Bulletin of Volcanology* 81, <https://doi.org/10.1007/s00445-019-1324-7>.
- Sottili, G., Palladino, D. M., Gaeta, M. & Masotta, M. 2012: Origins and energetics of maar volcanoes: examples from the ultrapotassic Sabatini Volcanic District (Roman Province, Central Italy). *Bulletin of Volcanology* 74, 163–186.
- Sottili, G., Palladino, D. M., Marra, F., Jicha, B., Karner, D. B. & Renne, P. 2010: Geochronology of the most recent activity in the Sabatini Volcanic District, Roman Province, Central Italy. *Journal of Volcanology and Geothermal Research* 196, 20–30.
- Sottili, G., Palladino, D. M. & Zanon, V. 2004: Plinian activity during the early eruptive history of the Sabatini volcanic district, Central Italy. *Journal of Volcanology and Geothermal Research* 135, 361–379.
- Sottili, G., Taddeucci, J., Palladino, D. M., Gaeta, M., Scarlato, P. & Ventura, G. 2009: Sub-surface dynamics and eruptive styles of maars in the Colli Albani Volcanic District, Central Italy. *Journal of Volcanology and Geothermal Research* 180, 189–202.
- Sulpizio, R., Zanchetta, G., Caron, B., Dellino, P., Mele, D., Giaccio, B., Insinga, D., Paterne, M., Siani, G., Costa, A., Macedonio, G. & Santacroce, R. 2014: Volcanic ash hazard in the Central Mediterranean assessed from geological data. *Bulletin of Volcanology* 76, 866, <https://doi.org/10.1007/s00445-014-0866-y>.
- Tamburrino, S., Insinga, D. D., Pelosi, N., Kissel, C., Laj, C., Capotondi, L. & Sprovieri, M. 2016: Tephrochronology of a ~ 70 ka-long marine record in the Marsili Basin (southern Tyrrhenian Sea). *Journal of Volcanology and Geothermal Research* 327, 23–39.
- Tamburrino, S., Insinga, D. D., Sprovieri, M., Petrosino, P. & Tiepolo, M. 2012: Major and trace element characterization of tephra layers offshore Pantelleria Island: insights into the last 200 ka of volcanic activity and contribution to the Mediterranean tephrochronology. *Journal of Quaternary Science* 27, 129–140.
- Tomlinson, E. L., Kinvig, H. S., Smith, V. C., Blundy, J. D., Gottsmann, J., Müller, W. & Menzies, M. A. 2012: The upper and lower Nisyros pumices: revisions to the Mediterranean tephrostratigraphic record based on micron-beam glass geochemistry. *Journal of Volcanology and Geothermal Research* 243, 69–80.
- Turbeville, B. N. 1992: $^{40}\text{Ar}/^{39}\text{Ar}$ ages and stratigraphy of the latera caldera, Italy. *Bulletin of Volcanology* 55, 110–118.
- Vakhrameeva, P., Koutsodendris, A., Wulf, S., Fletcher, W. J., Appelt, O., Knipping, M., Gertisser, R., Trieloff, M. & Pross, J. 2018: The cryptotephra record of the marine isotope stage 12 to 10 interval (460–335 ka) at Tenaghi Philippon, Greece: exploring chronological markers for the middle Pleistocene of the Mediterranean region. *Quaternary Science Reviews* 200, 313–333.
- Vakhrameeva, P., Koutsodendris, A., Wulf, S., Portnyagin, M., Appelt, O., Ludwig, T., Trieloff, M. & Pross, J. 2021: Land-sea correlations in the eastern Mediterranean region over the past c. 800 kyr based on macro- and cryptotephra from ODP site 964 (Ionian Basin). *Quaternary Science Reviews* 255, 106811, <https://doi.org/10.1016/j.quascirev.2021.106811>.
- Vakhrameeva, P., Wulf, S., Koutsodendris, A., Tjallingii, R., Fletcher, W. J., Appelt, O., Ludwig, T., Knipping, M., Trieloff, M. & Pross, J. 2019: Eastern Mediterranean volcanism during marine isotope stages 9 to 7 e (335–235 ka): insights based on cryptotephra layers at Tenaghi Philippon, Greece. *Journal of Volcanology and Geothermal Research* 380, 31–47.
- Villa, I. M. & Buettner, A. 2009: Chronostratigraphy of Monte vulture volcano (southern Italy): secondary mineral microtextures and ^{39}Ar - ^{40}Ar systematics. *Bulletin of Volcanology* 71, 1195–1208.
- Wagner, B., Tauber, P., Francke, A., Leicher, N., Binnie, S. A., Cvetkoska, A., Jovanovska, E., Just, J., Lacey, J. H., Levkov, Z., Lindhorst, K., Kouli, K., Krastel, S., Panagiotopoulos, K., Ulfers, A., Zaova, D., Donders, T. H., Grazhdani, A., Koutsodendris, A., Leng, M., Sadori, L., Schreinert, M., Vogel, H., Wonik, T., Zanchetta, G. & Wilke, T. 2022: The geodynamic and limnological evolution of Balkan Lake Ohrid, possibly the oldest extant lake in Europe. *Boreas*, <https://doi.org/10.1111/bor.12601>.
- Wagner, B. and 47 others 2019: Mediterranean winter rainfall in phase with African monsoons during the past 1.36 million years. *Nature* 573, 256–260.
- Wulf, S., Hardiman, M. J., Staff, R. A., Koutsodendris, A., Appelt, O., Blockley, S. P. E., Lowe, J., Manning, C. J., Ottolini, L., Schmitt, A. K., Smith, V. C., Tomlinson, E. L., Vakhrameeva, P., Knipping, M., Kotthoff, U., Milner, A. M., Müller, U. C., Christianis, K., Kalaitzidis, S., Tzedakis, P. C., Schmiel, G. & Pross, J. 2018: The marine isotope stage 1–5 cryptotephra record of Tenaghi Philippon, Greece: towards a detailed tephrostratigraphic framework for the eastern Mediterranean region. *Quaternary Science Reviews* 186, 236–262.
- Wulf, S., Keller, J., Paterne, M., Mingram, J., Lauterbach, S., Opitz, S., Sottili, G., Giaccio, B., Albert, P. G., Satow, C., Tomlinson, E. L., Viccaro, M. & Brauer, A. 2012: The 100–133 ka record of Italian explosive volcanism and revised tephrochronology of Lago Grande di Monticchio. *Quaternary Science Reviews* 58, 104–123.
- Wulf, S., Kraml, M., Brauer, A., Keller, J. & Negendank, J. F. W. 2004: Tephrochronology of the 100ka lacustrine sediment record of Lago Grande di Monticchio (southern Italy). *Quaternary International* 122, 7–30.
- Wulf, S., Kraml, M. & Keller, J. 2008: Towards a detailed distal tephrostratigraphy in the Central Mediterranean: the last 20,000 yrs record of Lago Grande di Monticchio. *Journal of Volcanology and Geothermal Research* 177, 118–132.
- Zanchetta, G., Bini, M., Di Vito, M.-A., Sulpizio, R. & Sadori, L. 2019: Tephrostratigraphy of paleoclimatic archives in Central Mediterranean during the bronze age. *Quaternary International* 499, 186–194.
- Zanchetta, G., Regattieri, E., Giaccio, B., Wagner, B., Sulpizio, R., Francke, A., Vogel, H., Sadori, L., Masi, A., Sinopoli, G., Lacey, J. H., Leng, M. J. & Leicher, N. 2016: Aligning and synchronization of MIS 5 proxy records from Lake Ohrid (FYROM) with independently dated Mediterranean archives: implications for DEEP core chronology. *Biogeosciences* 13, 2757–2768.

Supporting Information

Additional Supporting Information to this article is available at <http://www.boreas.dk>.

Fig. S1. Supplementary bixide plots of tephra layers TF-62/63 and the Magliano Roman Plinian Fall

(MRPF) deposits (A, B) and of tephra layers TF-66/-67/-68/-69/-71 and the Orvieto–Bagnoregio eruption (WOB) (C, D).

Fig. S2. TAS diagram, CaO/FeO vs. Cl and bioxide plots of tephra layers TF-64b/-65/-65a showing their geochemical similarities and potential origin from the Sabatini Volcanic District.

Fig. S3. Major element glass composition of TF-76/-78 compared with whole-rock XRF data of the Ponticello pumices (Nappi *et al.* 1995) and EPMA-WDS data of the BAG tephra (Pouclet *et al.* 1999).

Fig. S4. A–C. Supplementary bioxide plots of tephra layers TF-81/-82/-83/-84 discussed proximal data from the Rocamonfina volcano (RMF HKS lavas) and from Colli Albani volcanic district (Prata Porci, post Villa Senni (VS) lava flows Sincrotrone and Palazzolo, and Valmontone). S4D–E show bioxide plots of tephra layers TF-63(Population 2)/-64/-64a/-70/-72 and discussed Lower White Trachytic Tuff Units E and D together with data for the Bojano Basin (MOL10/14; BOJ-01).

Table S1. Analytical details of $^{40}\text{Ar}/^{39}\text{Ar}$ measurements.